Electronic Supplementary Material (ESI) for Journal of Materials Chemistry C.
This journal is © The Royal Society of Chemistry 2020

Supporting Information

Ultralong Organic Luminogens with Color-Tunability *via* Intermolecular Through-Space Charge-Transfer Characters

Yanju Luo,[ab] Zhenguo Pang,[a] Chuan Li,[a] Kuan Chen,[a] Xujun Zheng,*[a] Yan Huang[a] and Zhiyun Lu*[a]

[a] Key Laboratory of Green Chemistry and Technology (Ministry of Education), College of Chemistry, Sichuan University, Chengdu 610064 (P. R. China). E-mail: zhengxujun2019@gmail.com; luzhiyun@scu.edu.cn;

[b] Analytical & Testing Center, Sichuan University, Chengdu 610064 (P. R. China).

1) Experimental details

General Information

Materials. Unless otherwise described, all reagents and anhydrous solvents were purchased from commercial sources and used without further purification. All the solvents used in photophysical measurements were of analytical grades and freshly distilled prior to use. Carbazole (**Cz**) and 9,9-dimethylthioxanthene *S*,*S*-dioxide (**SO**) were purified through recrystallization from ethanol before used.

General method. ^{1}H NMR and ^{13}C NMR spectra were recorded on a Bruker AVANCE II-400 MHz spectrometer at 400 and 100 MHz in $CDCl_3$, respectively. Tetramethylsilane (TMS) was used as an internal standard. All chemical shift data were reported in the standard δ notation of parts per million. Splitting patterns were designed as follows: s (singlet), d (doublet), t (triplet) and m (multiplet). High resolution MS spectra were measured on a Q-TOF Premier ESI mass spectrometer (Micromass, Manchester, UK). The purity of target molecules was determined by high-performance liquid chromatography (Perkin-Elmer Flexar LC). Melting points were determined by a SG ERR melting point instrument without further correction. UV-vis spectra were measured on a Shimadzu UV-3600 spectrophotometer equipped with an integrating sphere. Absorption spectra for the solution samples were collected on a solution sample rack with quartz cell. Absorption spectra for the film and crystal samples were measured from an integrating sphere through reflective mode, in which the sample was located at the exit of the integrating sphere and a blank barium sulfate tablet was used to establish a zero baseline. Steady-state photoluminescence excitation and emission spectra were recorded on a Horiba Jobin Yvon Fluoromax-4 fluorescence spectrophotometer. Phosphorescence spectra of the solution and doped PMMA film samples at 77 K were measured on a Hitachi F-7000 fluorescence spectrophotometer, and phosphorescence spectra of the crystal samples at room temerature were measured on a Horiba Jobin Yvon Fluorolog-3 fluorescence spectrophotometer. Photoluminescence efficiency was collected on a Hamamatsu UV-NIR (C13534) absolute PL quantum yield spectrometer. Transient photoluminescence decay characteristics of the crystal samples were recorded on a Horiba Jobin Yvon FluoroHub-B equipped with a single photon counting controller. Single crystal X-ray diffraction data was obtained on a Xcalibur E X-ray single crystal diffractometer equipped with a graphite monochromator Mo-Kα (λ = 0.71073 Å) radiation. Two-photon excitated PL emission spectrum and corresponding photograph were recorded on a two-photon confocal

microscope (AIR MP+, Nikon, Japan). Photographs of the crystalline samples under UV and visible lights using a portable UV lamp (365 nm) and a blue lamp (420 nm) were taken by a mobile phone. Single crystal samples of **CzSO** and **β-CbSO** were both obtained by slow evaporation of saturated solution from mixed solvents (dichloromethane and ethanol) under room temperature. The crystallographic data for **CzSO** and **β-CbSO** reported here have been deposited in the Cambridge Structural Database with CCDC numbers of 1959108 and 1959109, respectively.

Computational method. Quantum chemistry calculations were performed on monomeric and dimeric **CzSO** and **β-CbSO** using Gaussian 09 software package with PBE0 functional and 6-311g (d) basis set. All calculation models for monomeric and dimeric **CzSO** and **β-CbSO** were extracted from their corresponding single crystal structures. To identify a better calculation method for these systems, the calculated vertical excitation energy data of monomeric **CzSO** and **β-CbSO** were compared with the corresponding experimental data derived from their maximal absorption in acetonitrile. The results indicated that the maximal absorption is 324 nm (3.83 eV) for **CzSO** and 336 nm (3.69 eV) for **β-CbSO** in acetonitrile; while the corresponding calculated vertical excitation energy data by PBE0 function is 327 nm (3.79 eV) for **CzSO** and 311 nm (3.99 eV) for **β-CbSO**. Since the calculated vertical excitation energy data are in good agreement with the experimental observations, the computation results should be reliable. Kohn-Sham frontier orbital analysis was subsequently performed to elucidate the mechanisms of possible singlet-triplet intersystem crossing (ISC), intermolecular charge transfer, and through-space conjugation as well in dimeric aggregates of **CzSO** and **β-CbSO**.

Preparation of droplet film sample of CzSO, and thermally fused film samples of CzSO and Cz:**SO blended mixture.** The droplet-film sample of **CzSO** was obtained by dropping the **CzSO** toluene solution (10 mg mL^{-1}) on a quartz substrate followed by slowly evaporation of the solvent at room temperature. For the thermally fused film sample of **CzSO**, it was obtained by heating a flask containing **CzSO** crystals and a quartz substrate at 260 ^{o}C to observe the complete melting of **CzSO** (Mp: 230 ^{o}C) under a nitrogen atmosphere, followed by slowly cooling down the flask to room temperature. For the thermally fused film sample of **Cz**:**SO** blended mixture, it was obtained by heating a flask containing a mixture of crystalline **Cz** and **SO** (1:1 in molar ratio) and a quartz substrate at 260 ^{o}C to observe the complete

melting of **Cz** (Mp: 245 °C) and **SO** (Mp: 160 °C) under a nitrogen atmosphere, followed by slowly cooling down the flask to room temperature.

Synthetic procedures and structural characterization data

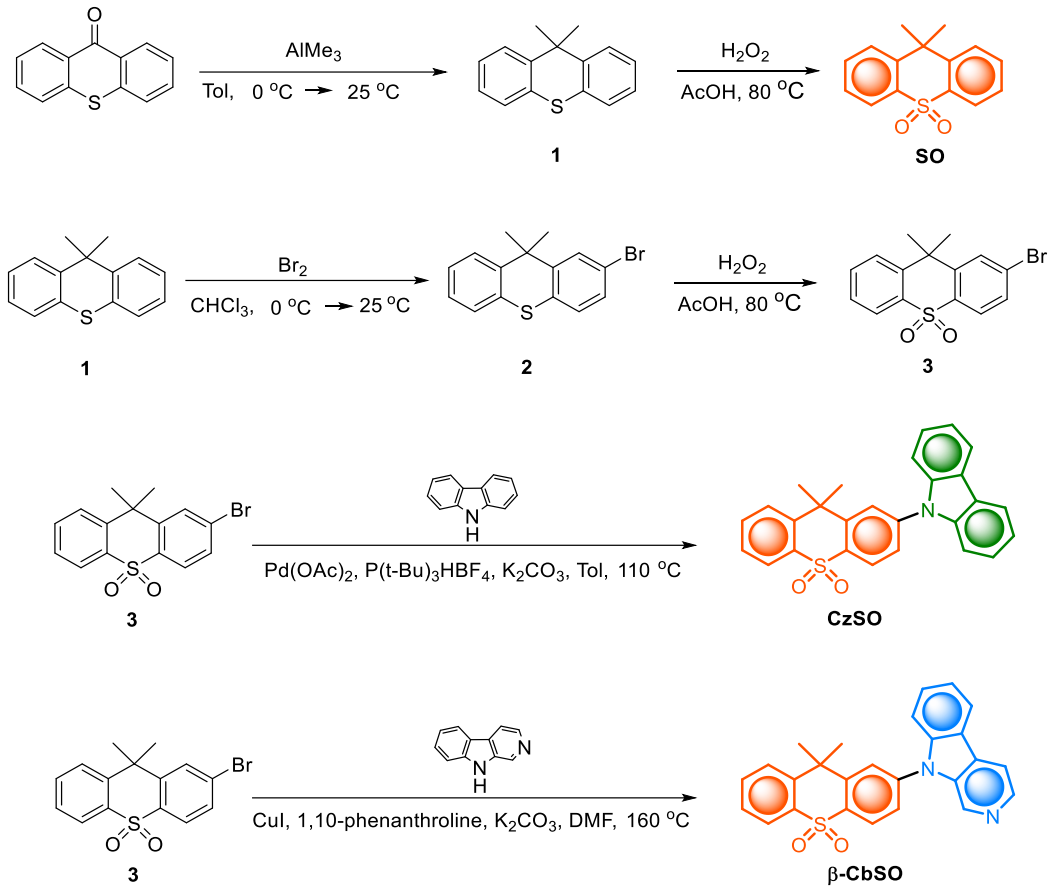

Scheme S1. Synthetic route to compounds **SO**, **CzSO** and **β-CbSO**.

Intermediates **1** and **2** were synthesized according to reported procedures.[1]

Synthesis of 2-bromo-9,9-dimethyl-9*H*-thioxanthene 10,10-dioxide (3) [1]

A solution of intermediate **2** (6.0 g, 19.70 mmol) in acetic acid (140 mL) was stirred at 80 °C for 0.5 h, then H_2O_2 (84 mL, 30 wt.% in H_2O) was added dropwise via a dropping funnel. After the addition, the mixture was refluxed for 2 h. After being cooled down to room temperature, the reaction mixture was cooled down, then poured into 60 mL water and extracted with CH_2Cl_2 (40 mL × 3). After the solvent was removed, the residue was purified using column chromatography on silica gel employing PE/CH_2Cl_2 (1/1) as an eluent to afford a white solid. Yield: 94%. Mp: 157-158 ℃. ^{1}H NMR (400 MHz, $CDCl_3$) δ (ppm): 8.18 (dd, J_1

= 7.6 Hz, J_2 = 0.8 Hz, 1 H), 8.05 (d, J = 8.4 Hz, 1H), 7.89 (d, J = 1.6 Hz, 1H), 7.74 (d, J = 8.0 Hz, 1H), 7.66 (dd, J_1 = 8.4 Hz, J_2 = 2.0 Hz, 1H), 7.64-7.58 (m, 1H), 7.52 (t, J = 7.6 Hz, 1H), 1.88 (s, 6H).

Synthesis of 9,9-dimethyl-9*H*-thioxanthene 10,10-dioxide (SO)

A solution of intermediate **1** (2.0 g, 8.84 mmol) in acetic acid (20 mL) was stirred at 80 ºC for 0.5 h, then H_2O_2 (28 mL, 30 wt.% in H_2O) was added dropwise via a dropping funnel. After the addition, the mixture was refluxed for 2 h. After being cooled down to room temperature, the precipitation was collected by filtration, and washed with water to afford the product. After being dried at 70 °C overnight, the product was obtained as a white solid. The white needle crystal was obtained by recrystallization in ethanol. Yield: 94%. Mp: 160-162 ℃. ^{1}H NMR (400 MHz, $CDCl_3$) δ (ppm): 8.20 (dd, J_1 = 7.6 Hz, J_2 = 1.6 Hz, 2H), 7.75 (dd, J_1 = 8.0 Hz, J_2 = 0.8 Hz, 2H), 7.60 (m, 2H), 7.51 (td, J_1 = 8.0 Hz, J_2 = 1.2 Hz, 2H), 1.89 (s, 6 H).

Synthesis of 2-(9*H*-carbazol-9-yl)-9,9-dimethyl-9*H*-thioxanthene 10,10-dioxide (CzSO)

A flask was charged with 9*H*-carbazole (0.16 g, 0.98 mmol), intermediate **3** (0.30 g, 0.89 mmol), $Pd(OAc)_2$ (4.0 mg, 0.018 mmol), P(*t*-Bu)$_3$•HBF_4 (10.3 mg, 0.036 mmol), K_2CO_3(0.25 g, 1.8 mmol) and dry toluene (6 mL), and the reaction mixture was stirred at 110 ºC for 24 h under argon. Then the reaction mixture was cooled down, then poured into 30 mL of water and extracted with CH_2Cl_2 (20 mL × 3). The resultant organic phase was washed with brine, and dried over anhydrous Na_2SO_4. After the solvent was removed in vacuum, the residue was purified using column chromatography on silica gel employing PE/CH_2Cl_2 (1/1) as the eluent to afford a white solid. Yield: 85%. Mp: 230-231 ℃. ^{1}H NMR (400 MHz, $CDCl_3$) δ (ppm): 8.44 (d, J = 8.0 Hz, 1H), 8.26 (dd, J_1 = 7.6 Hz, J_2 = 1.2 Hz, 1H), 8.17-8.15 (m, 2H), 7.99 (d, J = 1.6 Hz, 1H), 7.80-7.74 (m, 2H), 7.65 (td, J_1 = 7.6 Hz, J_2 = 1.6 Hz, 1H), 7.56 (td, J_1 = 7.6 Hz, J_2 = 0.8 Hz, 1H), 7.47-7.41 (m, 4H), 7.36-7.32 (m, 2H), 1.94 (s, 6H). ^{13}C NMR (100 MHz, $CDCl_3$) δ (ppm): 148.3, 145.4, 141.9, 140.2, 136.7, 135.2, 133.1, 127.8, 126.4, 126.4, 125.8, 125.6, 124.4, 123.9, 120.9, 120.6, 109.5, 39.6, 31.0. HRMS (ESI) m/z for $C_{27}H_{21}NO_2SNa^+$ [M + Na]$^+$ Calcd.: 446.1185, found: 446.1179.

Synthesis of 9,9-dimethyl-2-(9*H*-pyrido[3,4-*b*]indol-9-yl)-9*H*-thioxanthene 10,10-dioxide (β-CbSO)

A flask was charged with 9*H*-pyrido[3,4-*b*]indole (226 mg, 1.34 mmol), intermediate **3** (378 mg, 1.12 mmol), CuI (43 mg, 0.22 mmol), 1,10-phenanthroline (44 mg, 0.22 mmol), K_2CO_3 (619 mg, 4.5 mmol) and dry DMF (5 mL), and the reaction mixture was stirred at 160 ºC for

34 h under argon. The reaction mixture was cooled down, then poured into 15 mL brine, the precipitate was filtered under reduced pressure, then was subject to column chromatography (eluent: Tol/DCM/MeOH = 20/20/1) to afford a yellow solid. Yield: 61%. Mp: 269-270 ℃. ^{1}H NMR (400 MHz, $CDCl_3$) δ (ppm): 8.91 (s, 1H), 8.58 (d, *J* = 5.6 Hz, 1H), 8.48 (d, *J* = 8.4 Hz, 1H), 8.28-8.23 (m, 2H), 8.07 (d, *J* = 5.2 Hz, 1H), 8.01 (d, *J* = 2.0 Hz, 1H), 7.81-7.78 (m, 2H), 7.69-7.56 (m, 3H), 7.52 (d, *J* = 8.4 Hz, 1H), 7.42 (t, *J* = 8.0 Hz, 1H), 1.96 (s, 6H). ^{13}C NMR (100 MHz, $CDCl_3$) δ (ppm): 148.7, 145.3, 141.1, 140.8, 140.3, 136.5, 136.0, 133.3, 132.3, 130.0, 129.4, 127.9, 126.7, 125.8, 125.4, 124.5, 123.8, 122.2, 122.0, 121.7, 114.9, 110.3, 39.7, 31.1. HRMS (ESI) m/z for $C_{26}H_{20}N_2O_2SH^+$ $[M+H]^+$ Calcd.: 425.1318, found 425.1298; $C_{26}H_{20}N_2O_2SNa^+$ $[M + Na]^+$ Calcd.: 447.1138, found: 446.1081.

2) Characterization results

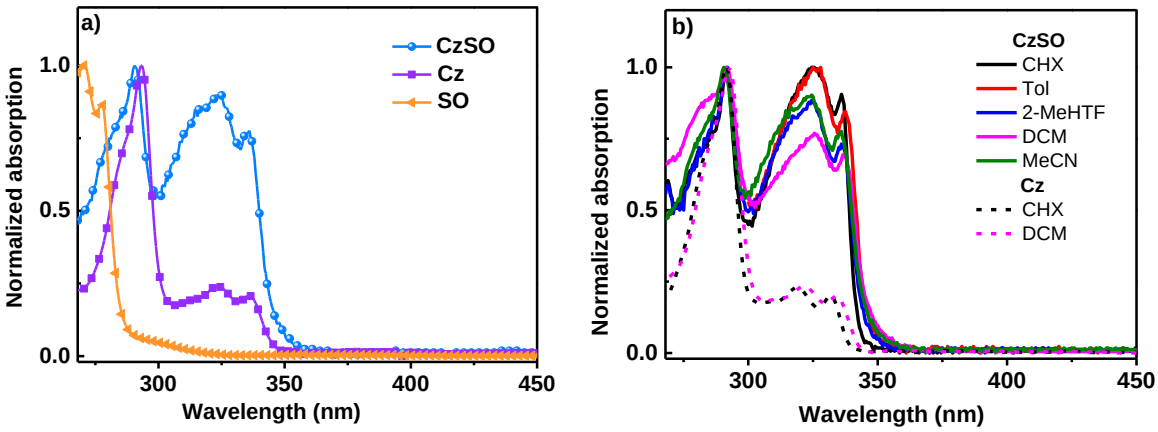

Figure S1. a) Normalized absorption spectra of **CzSO**, **Cz** and **SO** in dilute MeCN solution. b) Normalized absorption spectra of **CzSO** and **Cz** in solvents with different polarity. CHX: cyclohexane; Tol: toluene; 2-MeTHF: 2-methyltetrahydrofuran; DCM: dichloromethane; MeCN: acetonitrile.

The absorption onset of **CzSO** solution is slightly red-shifted than that of **Cz**, indicative of the presence of weak electron coupling between **Cz** and **SO** moieties in **CzSO** in the ground state.

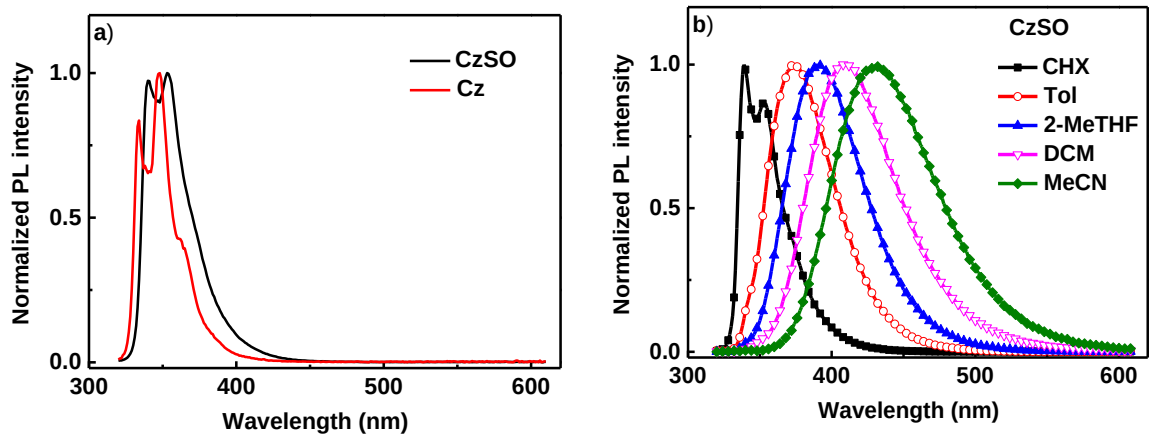

Figure S2. a) Normalized photoluminescence (PL) emission spectra of **CzSO** and **Cz** in CHX solution. b) Normalized PL emission spectra of **CzSO** in solvents with different polarity under ambient conditions (λ_{ex} = 310 nm, 10^{-5} M).

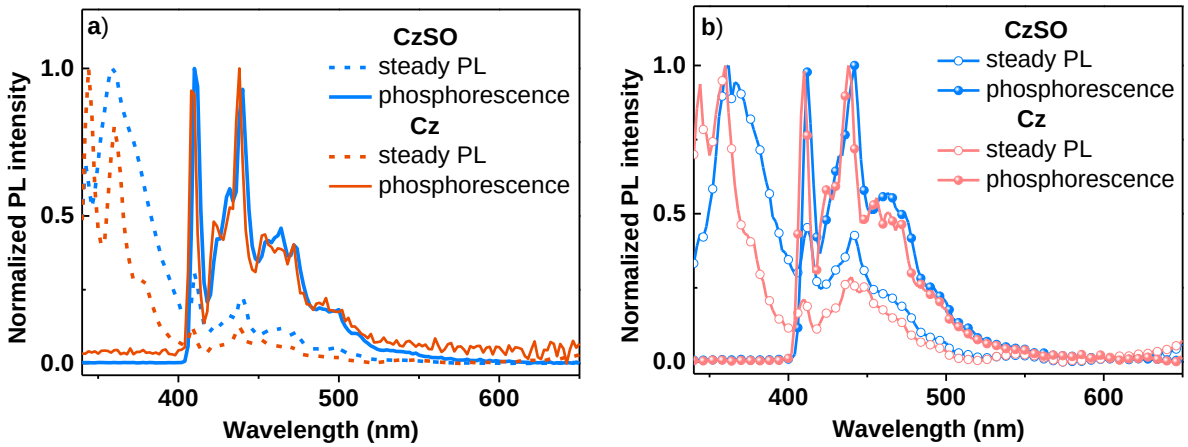

Figure S3. Steady-state PL spectra and phosphorescence spectra (40 Hz delayed) of **CzSO** and **Cz** at 77 K. a) In 2-MeTHF solution (10^{-5} M, λ_{ex} = 330 nm). b) In 1 wt.%-doped PMMA film (λ_{ex} = 330 nm).

According to the phosphorescence spectrum of **Cz**, the triplet energy level of isolated **Cz** is determined to be 3.02 eV in both 2-MeTHF and PMMA matrix.

Table S1. Structure data of **CzSO** and **β-CbSO** single crystals.

Name	**CzSO**	**β-CbSO**
Empirical formula	$C_{27}H_{21}NO_2S$	$C_{26}H_{20}N_2O_2S$
Formula weight	423.51	424.50
Temperature (K)	293.15	293.15
Crystal system	monoclinic	monoclinic
Space group	$P2_1/c$	$P2_1/c$
a (Å)	18.1383(19)	8.5006(4)
b (Å)	7.9990(6)	31.1202(15)
c (Å)	15.0009(15)	7.6409(4)
α ( )	90	90
β ( )	106.602(11)	90.895(5)
γ ( )	90	90
Volume ($Å^3$)	2085.7(4)	2021.08(17)
Z	4	4
Density (g/cm^3)	1.349	1.395
μ (mm^{-1})	0.180	0.188
F(000)	888.0	888.0
Crystal size (mm^3)	0.35 ×0.3 ×0.25	0.4 ×0.35 ×0.25
Radiation	MoK*α* (λ = 0.71073)	MoK*α* (λ = 0.71073)
2Θ range for data collection/°	6.238 to 58.13	5.94 to 52.744
Index ranges	-22 ≤ h ≤ 24, -10 ≤ k ≤ 7, -20 ≤ l ≤ 20	-10 ≤ h ≤ 9, -38 ≤ k ≤ 31, -9 ≤ l ≤ 9
Reflections collected	10586	10730
Independent reflections	4803 [R_{int} = 0.0222, R_{sigma} = 0.0381]	4032 [R_{int} = 0.0225, R_{sigma} = 0.0335]
Data/restraints/parameters	4803/0/282	4032/0/282
Goodness-of-fit on F^2	1.027	1.029
Final *R* indexes [$I>=2\sigma$ (I)]	R_1 = 0.0487, wR_2 = 0.1135	R_1 = 0.0460, wR_2 = 0.1030
Final *R* indexes [all data]	R_1 = 0.0770, wR_2 = 0.1308	R_1 = 0.0640, wR_2 = 0.1153
Largest diff. peak/hole (e $Å^{-3}$)	0.29/-0.26	0.29/-0.37

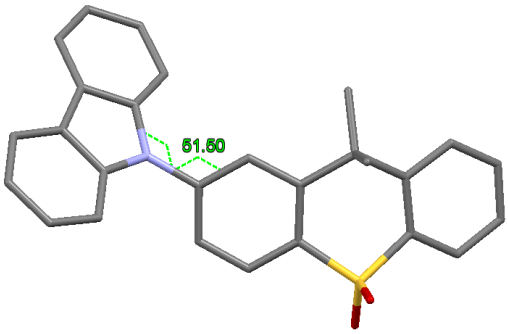

Figure S4. The molecular structure of **CzSO** extracted from its crystallographic structure. The torsion angle between the **Cz** and **SO** units (51.50º) is indicated by green dashed lines.

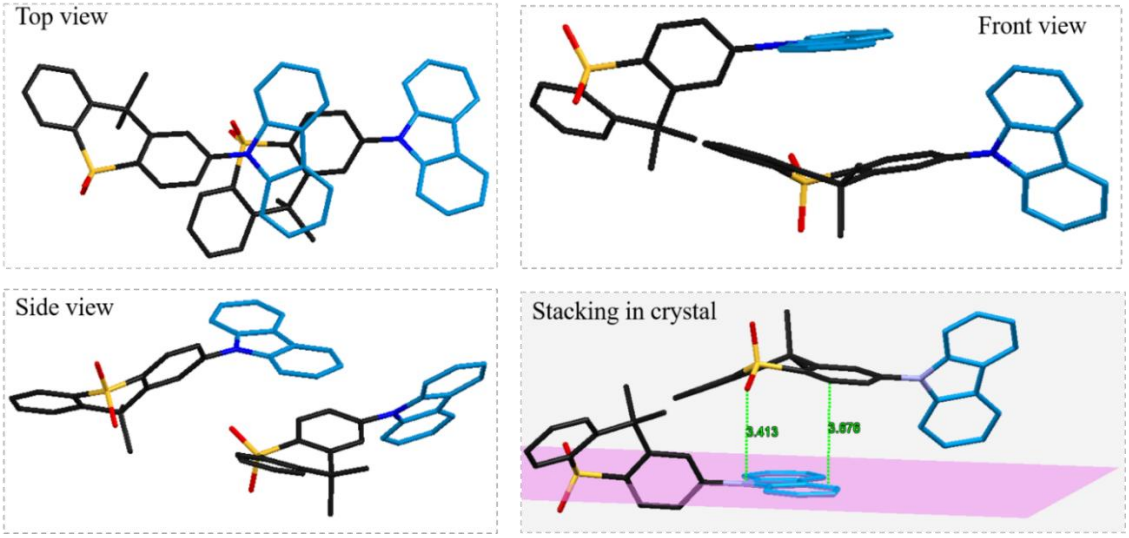

Figure S5. Molecular stacking in **CzSO** single crystal. The shortest distance from **SO** (oxygen atom) to **Cz** (nitrogen atom) is 3.413 Å.

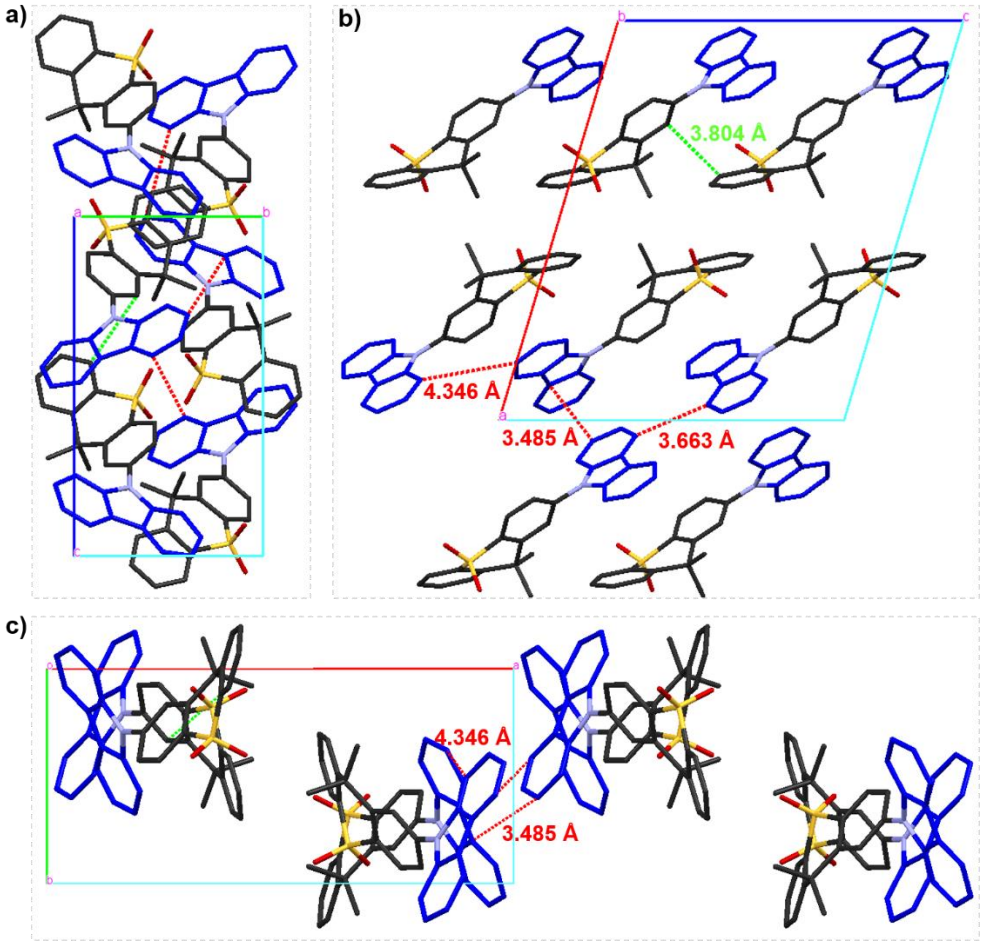

Figure S6. Molecular packing in the crystal lattice of **CzSO**. View down: a) the a-axis; b) the b-axis; and c) the c-axis, respectively.

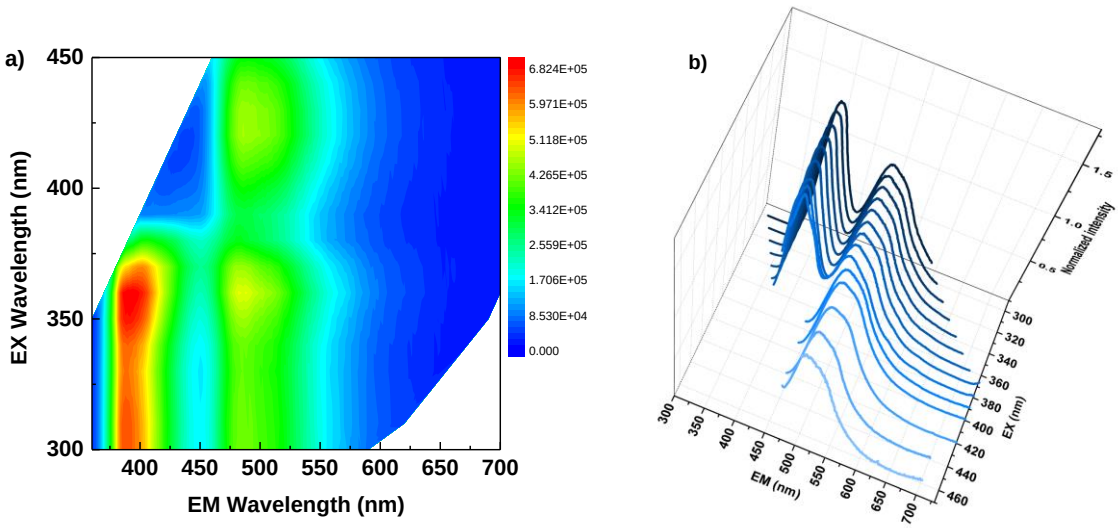

Figure S7. a) Steady state excitation-emission mapping of **CzSO** crystal. b) Normalized steady-state PL spectra of **CzSO** crystal upon excitation at 300, 310, 320, 330, 340, 350, 360, 370, 380, 390, 400, 420, 440 and 460 nm under ambient conditions.

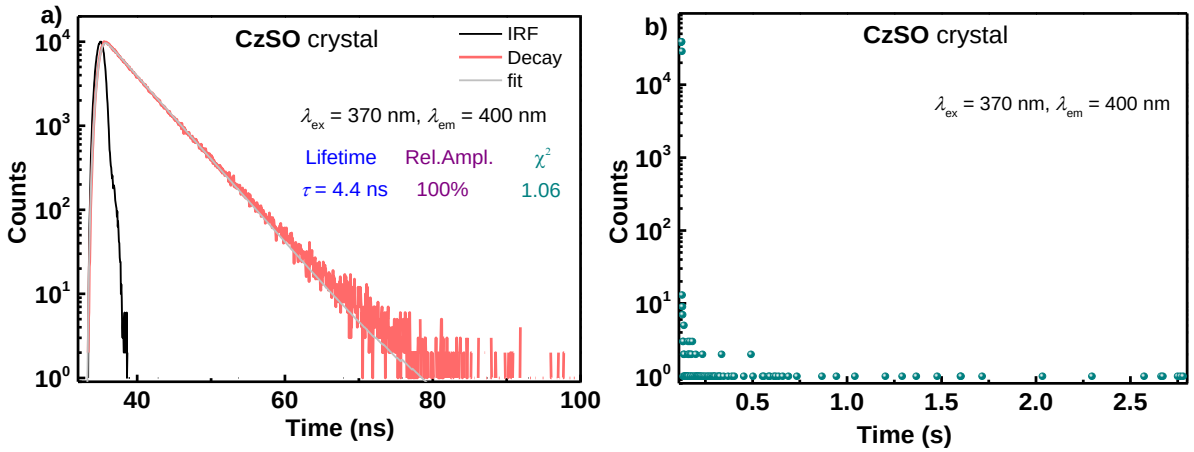

Figure S8. PL decay profiles of the higher-energy emission band of crystalline **CzSO** recorded at λ_{em} = 400 nm under ambient conditions (λ_{ex} = 370 nm) at different time-range windows of: a) 200 ns; and b) 5.6 s. Note that for the higher-energy PL band (λ_{PL} = 400 nm), only short-lived species in nanosecond scale could be detected.

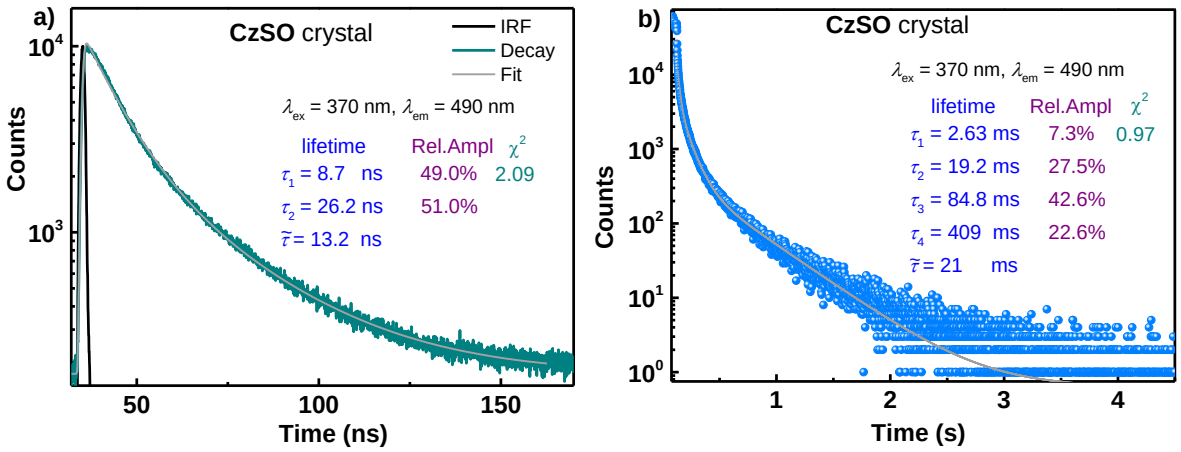

Figure S9. PL decay profiles of the lower-energy PL emission band of crystalline **CzSO** recorded at λ_{em} = 490 nm under ambient conditions (UV-light excitation, λ_{ex} = 370 nm) at different time-range windows of: a) 200 ns; and b) 5.6 s.

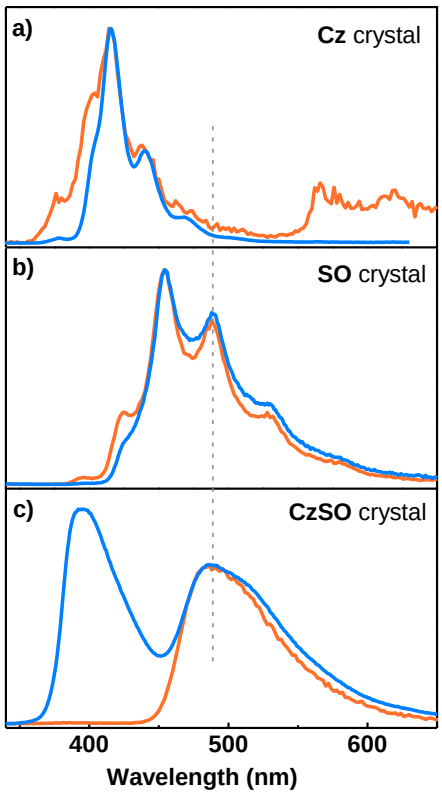

Figure S10. Steady state (blue line) and delayed PL spectra (orange line, delay time: 0.1 ms) of: a) **Cz** crystal; b) **SO** crystal, and c) **CzSO** crystal samples. (λ_{ex} = 330 nm).

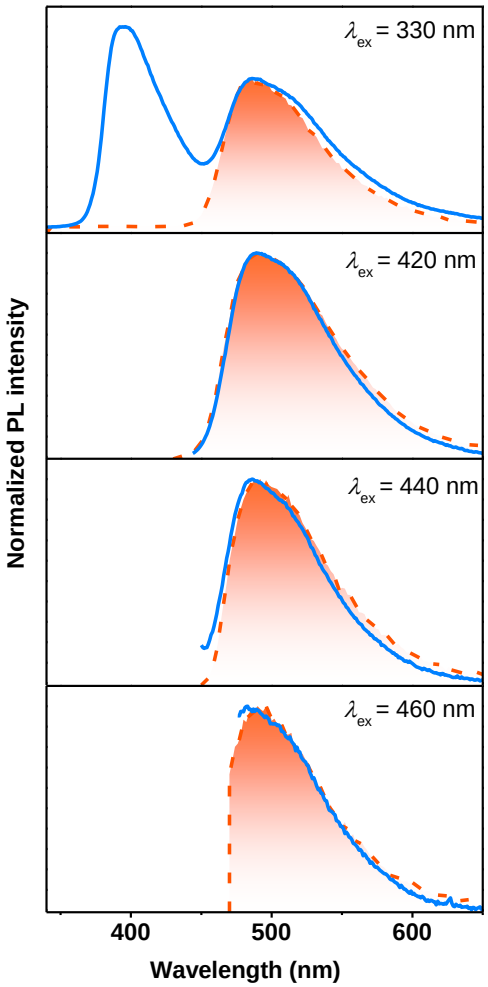

Figure S11. Steady state PL spectra (blue line) and delayed PL spectra (orange filled area, delay time: 0.1 ms) of crystalline **CzSO** under different excitation at 330 nm, 420 nm, 440 nm and 460 nm, respectively.

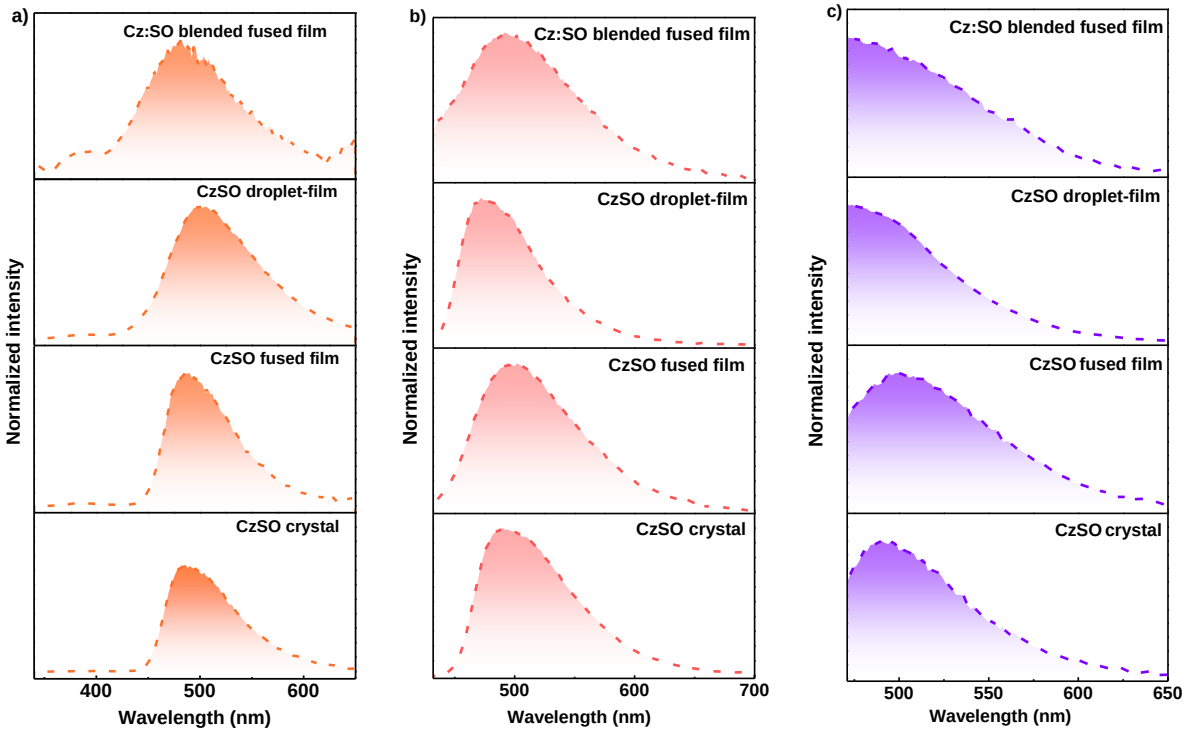

Figure S12. Delayed PL spectra (delay time = 0.1 ms) of thermally fused **Cz**:**SO** blend film, **CzSO** droplet-film, thermally fused **CzSO** film and crystalline **CzSO** under excitation of: a) 330 nm; b) 420 nm; and c) 460 nm.

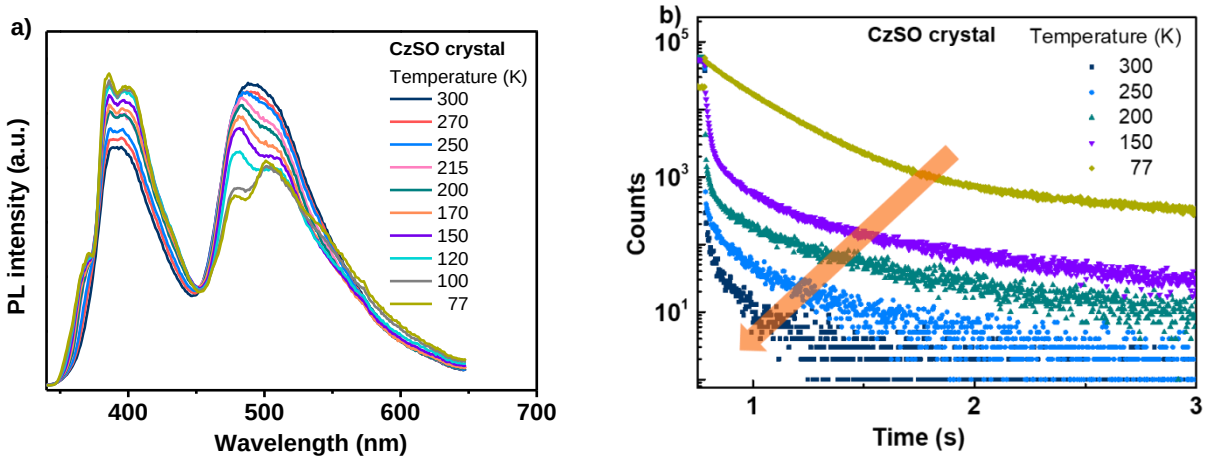

Figure S13. a) Temperature-dependent PL spectra of crystalline **CzSO** under N_2 (λ_{ex} = 330 nm). b) Temperature-dependent PL decay profiles of crystalline **CzSO** at λ_{em} of 510 nm under N_2 (λ_{ex} = 355 nm).

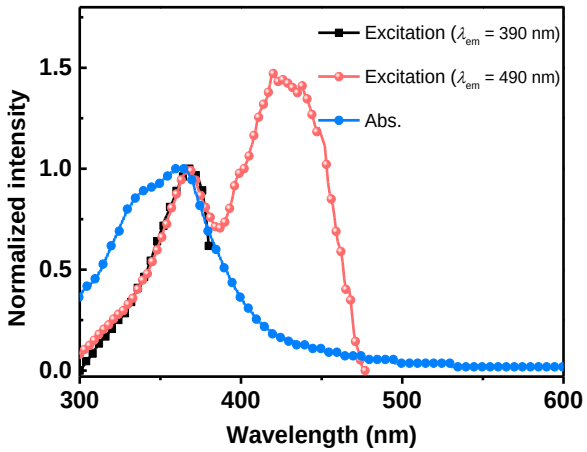

Figure S14. Absorption and PL excitation spectra (λ_{em} = 390, 490 nm) of crystalline **CzSO** at ambient conditions.

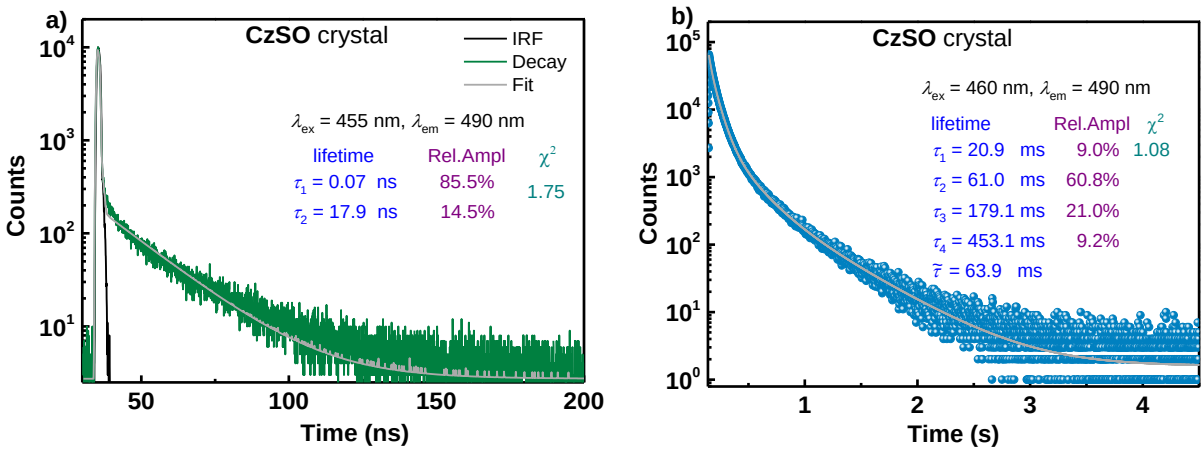

Figure S15. PL decay profiles of the lower-energy emission band of crystalline **CzSO** recorded at λ_{em} = 490 nm under ambient conditions (visible light excitation, λ_{ex} = 455 or 460 nm) at different time-range windows of: a) 200 ns; and b) 5.6 s.

After careful comparison between the PL decay and IRF curves, we conjectured that the species with the shortest lifetime (τ < 1 ns) in Figure S15a may originate from the excitation source (nano-diode 455 nm) due to the light scattering.

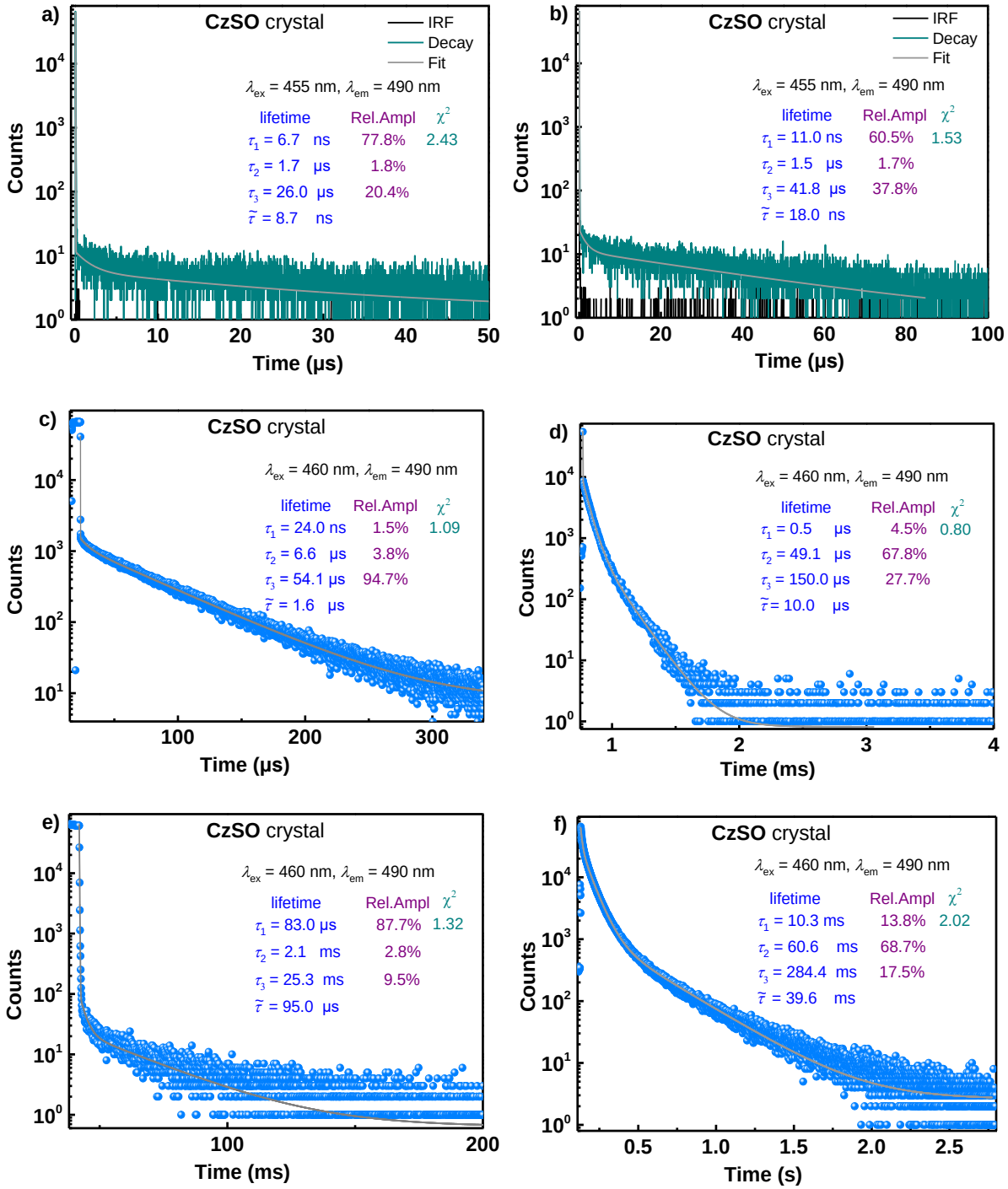

Figure S16. PL decay profiles of the lower-energy PL emission band of crystalline **CzSO** recorded at λ_{em} = 490 nm under ambient conditions (visible light excitation, λ_{ex} = 455 or 460 nm) at different time-range windows of: a) 50 µs; b) 100 µs; c) 340 µs; d) 11 ms; e) 350 ms; and f) 2.8 s.

According to Figure S9b, crystalline **CzSO** is observed to show four-exponential PL decay functions with lifetimes of τ_1, τ_2, τ_3 and τ_4, respectively. Despite the fact that short-lived

species are all discernable in different measurement time-range windows of 50 μs, 100 μs, 340 μs, 11 ms, 350 ms and 2.8 s, respectively, the lifetime data of these short-lived species in crystalline **CzSO** are always shorter than 20 ms (Figure S16). Therefore, for the PL decay curves shown in Figure S9b (under UV excitation), the two species with shorter lifetime data of τ_1 (2.6 ms) and τ_2 (19.2 ms) can be safely assigned to prompt photoluminescence species containing all the short-lived PL components in crystalline **CzSO**, and the other two species with longer lifetime data of τ_3 (84.8 ms) and τ_4 (409 ms) should be assigned to long-lived PL species.

Similarly, according to the PL decay curves shown in Figure S15 (under visible excitation), the relatively short-lived species with lifetime of τ_1 (20.9 ms) should be assigned to the prompt PL species which contains all the short-lived PL components; while the other three lifetime species with longer lifetime data of τ_2 (61.0 ms), τ_3 (179.1 ms) and τ_4 (453.1 ms) should be assigned to the long-lived PL species in crystalline **CzSO**.

Table S2. Persistent emission efficiencies of crystalline **CzSO** under ambient conditions.

Compd.	λ_{ex} (nm)	λ_{em} (nm)	$\varphi_{PL,total}$ (%)	$\varphi_{PL(490\text{ or }460\text{ nm})}$ (%)	φ_{UOL} (%)
CzSO	330	396, 490	35	14.0[a)]	9.1
	440	490	-	28.9	26.3
β-CbSO	330	384, 460	4.9	3.0[a)]	1.5
	440	460	-	5.4	4.4

[a)] The PL quantum efficiency data (φ_{PL}) of the emission band centered at 490 nm for **CzSO** crystals, and 460 nm for **β-CbSO** crystals under UV-light excitation at 330 nm are determined through peak differentation-imitating analysis from the corresponding steady-state PL spectra.

Using the relative amplitude data (*f*) of the τ_3 and τ_4 components, the fraction of UOL (φ_{UOL}) in crystalline **CzSO** is extracted from the total φ_{PL} data according to equation (1). The results indicate that the corresponding φ_{UOL} data of crystalline **CzSO** is 9.1% under UV excitation, and 26.3% under visible excitation. Similarly, the φ_{UOL} in crystalline **β-CbSO** is extracted from the corresponding total φ_{PL} according to equation (1) by using the corresponding *f* data of the long-lived emission components in crystalline **β-CbSO** sample.

$$\varphi_{UOL} = f_{UOL} \times \varphi_{PL} \qquad (1)$$

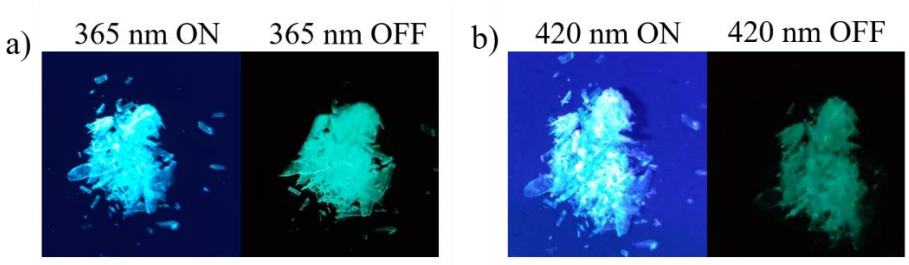

Figure S17. Photographs of crystalline **CzSO** under irradiation ON/OFF of: a) 365 nm; and b) 420 nm.

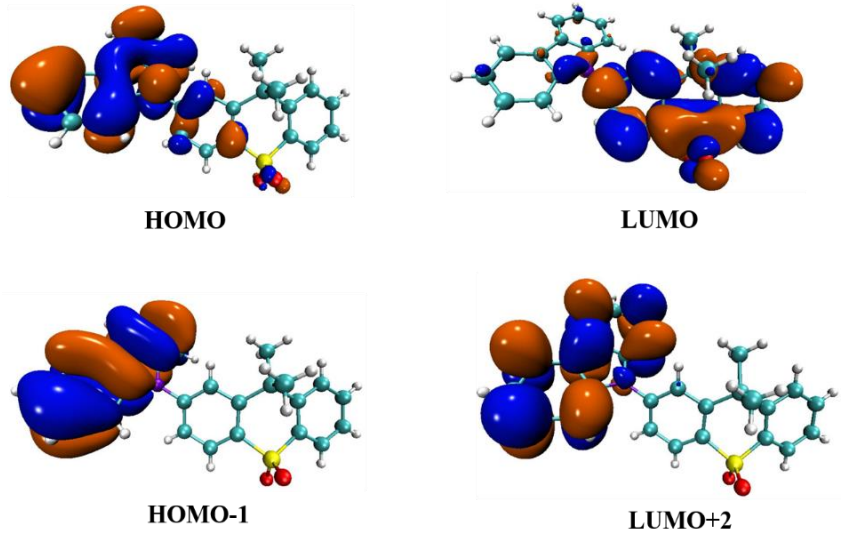

Figure S18. Calculated electron cloud distributions of HOMO, HOMO-1, LUMO and LUMO+2 orbitals of monomeric **CzSO** (isovalue is 0.02).

Table S3. The singlet and triplet excited state transition configurations of monomeric **CzSO** revealed by TD-DFT calculations (isovalue is 0.02).

monomeric **CzSO**					
	Transition configuration	CI	Transition Character	*f*	Δ*E*
S_0-S_1	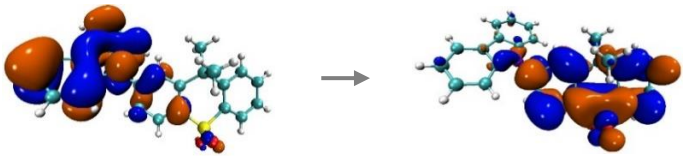	93.8%	intramolecular CT	0.165	3.790 eV
S_0-S_2	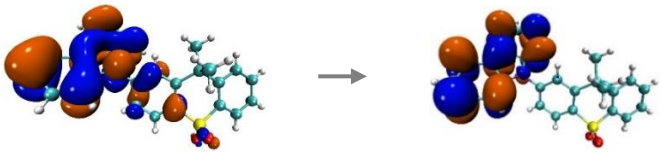	91.6%	$LE_{(Cz)}$	0.052	4.164 eV
S_0-S_3	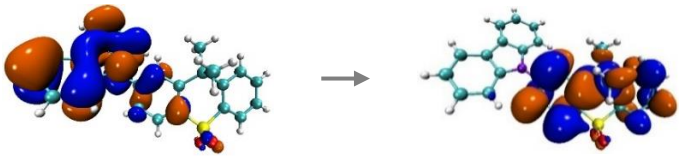	89.2%	intramolecular CT	0.002	4.199 eV
S_0-S_4	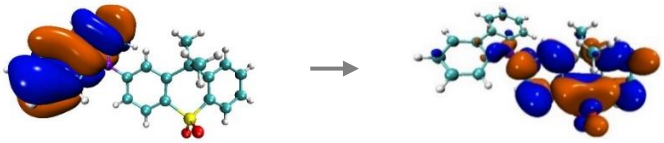	92.7%	intramolecular CT	0.001	4.204 eV
S_0-S_5		93.3%	intramolecular CT	0.020	4.620 eV
S_0-S_6	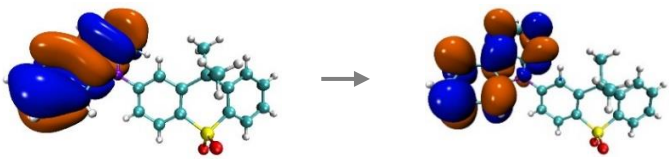	74.6%	$LE_{(Cz)}$	0.121	4.656 eV
S_0-T_1	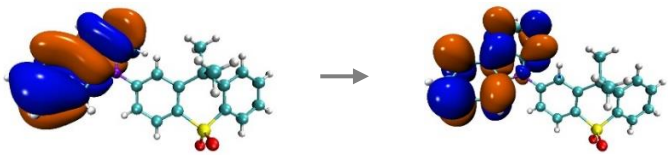	70.8%	$LE_{(Cz)}$	0.000	3.120 eV
S_0-T_2	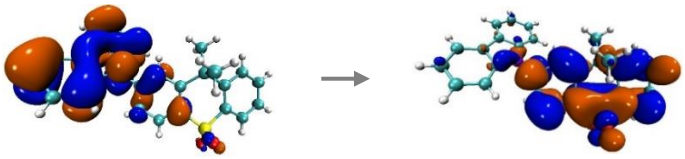	48.7%	intramolecular CT	0.000	3.255 eV
S_0-T_3	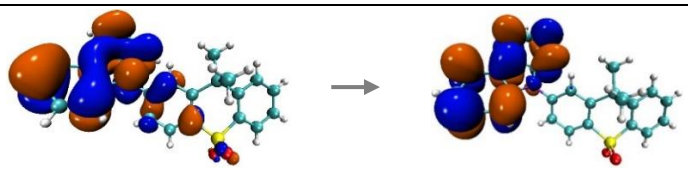	81.3%	$LE_{(Cz)}$	0.000	3.422 eV

Table S4. The singlet and triplet excited state transition configurations of monomeric **CzSO** revealed by TD-DFT calculations. The matched triplet excited states that contain the same orbital transition components of S_1 were highlighted in red.

	n-th	Energy (eV)	Transition configuration (%)
S_n	1	3.790	H→L (93.8)
T_n	1	3.120	H-2→L+2 (5.0), H-1→L+2 (70.8), H-1→L+3 (1.0), H→L+5 (13.1), H-1→L+6 (1.2)
	2	3.255	H-6→L+4 (1.5), H-5→L+3 (2.3), H-4→L (5.1), H→L (48.7), H→L+2 (6.2)
	3	3.422	H-6→L+1 (1.6), H-5→L (1.2), H-2→L+5 (3.9), H→L+2 (81.3), H→L+3 (1.1)
	4	3.586	H-9→L (1.3), H-9→L+3 (1.7), H-6→L+4 (3.6), H-3→L (16.1), H-3→L+3 (21.1)
	5	3.902	H-7→L+2 (1.2) , H-6→L (1.3), H-6→L+1 (22.2), H-5→L (5.6), H-4→L+1 (5.6), H-3→L (1.5), H-2→L+5 (2.1), H→L (28.4)
	6	3.994	H-4→L+1 (1.6), H-1→L+2 (0.9), H→L+1 (77.8)
	7	4.070	H-2→L (1.2), H-2→L+2 (5.2), H-1→L+3 (1.9), H-1→L+6 (1.7), H→L+1 (2.4), H→L+5 (35.7)
	8	4.148	H-2→L+2 (8.3), H→L (59.7), H→L+5 (17.3)

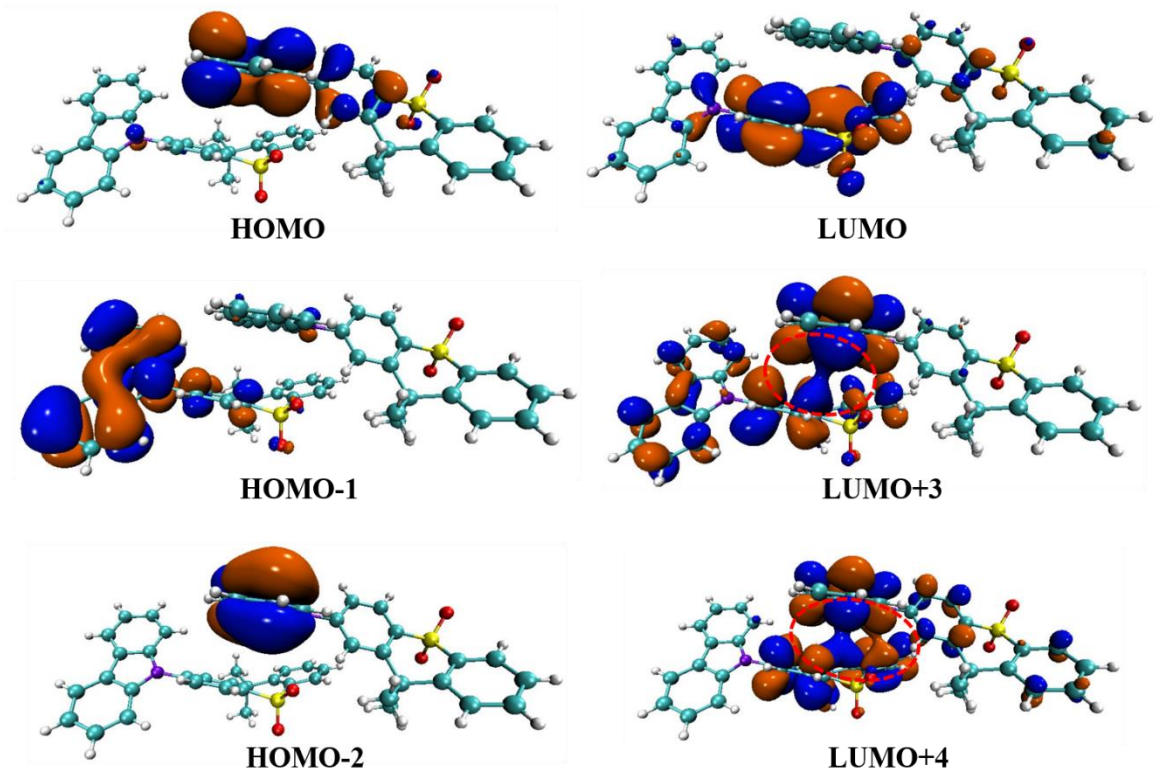

Figure S19. Calculated electron cloud distribution of HOMO, HOMO-1, HOMO-2, LUMO, LUMO+3 and LUMO+4 orbitals of dimeric **CzSO** aggregates (isovalue is 0.02).

Table S5. The singlet excited state transition configurations of dimeric **CzSO** aggregates revealed by TD-DFT calculations (isovalue is 0.02).

dimeric **CzSO**					
	Transition configuration	CI	Transition Character	*f*	Δ*E*
S_0-S_1		97.2%	**intermolecular CT**	0.003	3.765 eV
S_0-S_2		81.7%	intramolecular CT	0.259	3.819 eV
S_0-S_3		78.2%	intramolecular CT	0.066	3.837 eV
S_0-S_4		49.6%	**intermolecular CT** + $LE_{(Cz)}$	0.052	4.100 eV
S_0-S_5		89.7%	**intermolecular CT**	0.010	4.108 eV
S_0-S_6		78.3%	**intermolecular CT** + $LE_{(Cz)}$	0.051	4.149 eV

Table S6. The singlet and triplet excited state transition configurations of dimeric **CzSO** aggregates revealed by TD-DFT calculations. The matched triplet excited states that contain the same orbital transition components of S_1 were highlighted in red.

	n-th	Energy (eV)	Transition configuration (%)
S_n	1	3.765	H→L (97.2)
T_n	1	3.119	H-2→L+2 (7.6), H-2→L+3 (32.2), H-2→L+4 (21.1), H-2→L+8 (1.0), H→L+11 (12.2)
	2	3.120	H-2→L+2 (7.6), H-15→L+14 (4.0), H-5→L+2 (3.9), H-5→L+12 (2.8), H-3→L+2 (62.8), H-3→L+6 (1.0)
	3	3.263	H-11→L+5 (3.6), H-10→L+1 (5.0), H-10→L+7 (2.1), H-7→L+1 (3.7), H-6→L+1 (1.1), H→L+1 (37.5), H→L+3 (4.8), H→L+4 (4.0), H→L+7 (6.6)
	4	3.270	H-13→L (1.8), H-12→L (1.7), H-11→L (1.7), H-1→L (39.1), H-1→L+1 (1.8), H-1→L+2 (4.2), H→L (1.3), H→L+1 (1.3)
	5	3.388	H-4→L+15 (1.2), H→L (0.3), H→L+2 (8.8), H→L+3 (35.6), H→L+4 (22.3)
	6	3.414	H-9→L(1.8), H-5→L+14 (1.2), H-1→L+2 (69.1), H-1→L+6 (1.1), H→L+2 (1.9)
	7	3.568	H-13→L(1.2), H-12→L(5.0), H-12→L+3 (1.4), H-12→L+9 (3.2), H-12→L+8 (6.5), H-11→L (2.3), H-9→L (7.1), H-9→L+3 (2.6), H-9→L+6 (6.9), H-9→L+8 (4.4), H-8→L+8 (8.1), H-8→L+8 (8.1), H-7→L+8 (3.6), H→L (3.6)
	8	3.588	H-12→L+9 (1.2), H-10→L+7 (2.5), H-10→L+9 (5.8), H-8→L+7 (4.8), H-8→L+9 (2.4), H-7→L+1 (2.9), H-7→L+5 (3.3), H-6→L+1 (9.8), H-6→L+9 (8.5)
	9	3.773	H→L (84.3), H→L+1 (3.5)
	10	3.910	H-15→L+2 (1.2), H-14→L+4 (0.8), H-13→L+4 (8.0), H-13→L+5 (3.2), H-13→L+8 (3.0), H-12→L+3 (1.3), H-9→L (5.3), H-3→L+14 (1.5), H-1→L (27.1), H→L (1.5)
	11	3.924	H-12→L+5 (4.4), H-12→L+9 (1.6), H-7→L+5 (2.2), H→L (0.03), H→L+1 (29.3), H→L+13 (4.2)
	12	4.028	H-10→L+5 (1.7), H-4→L+3 (1.7), H-4→L+4 (1.3), H-2→L+1 (1.7), H-2→L+3 (4.5), H-2→L+4 (2.9), H→L+3 (3.0), H→L+9 (6.4)
	13	4.040	H-3→L+2 (4.9), H-1→L+2 (3.3), H-1→L+3 (23.8), H-1→L+10 (10.4), H→L+3 (1.3)
	14	4.057	H-10→L+11 (1.0), H-2→L (19.0), H→L+5 (23.1), H→L+9 (3.4), H→L+11 (19.2)
	15	4.078	H-5→L+3 (1.5), H-3→L (8.5), H-3→L+2 (13.8), H-1→L+4 (6.6), H-1→L+10 (34.8), H→L+10 (1.1)

The calculated results indicated that the electronic transitions from the ground state (S_0) to the first excited singlet state (S_1) for monomeric and dimeric **CzSO** are mainly derived from the highest occupied molecular orbital (HOMO) to the lowest unoccupied molecular orbital (LUMO). Energy levels of the possible T_n states with ± 0.3 eV range relative to the S_1 were illustrated in Figure 2c, and T_n states with the same transition orbital compositions as S_1 state were also indicated because they are the main elements for the intersystem crossing process from S_1 to T_n states.[12]

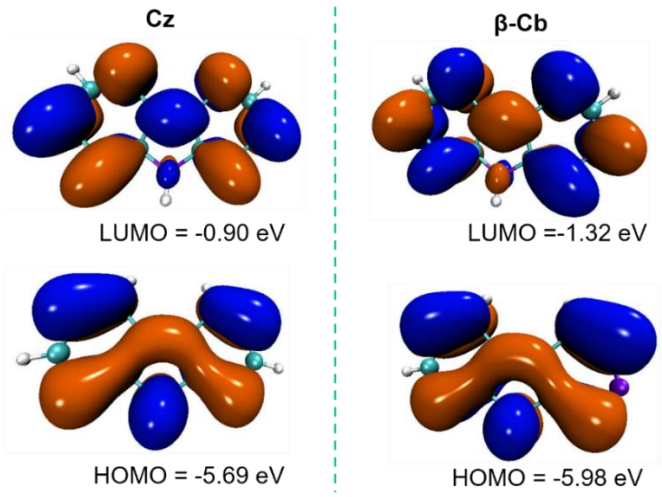

Figure S20. The calculated electron cloud distribution and energy levels of HOMO and LUMO orbitals of **Cz** and **β-Cb** (B3LYP functional and 6-311g (d, p) basis, isovalue is 0.02).

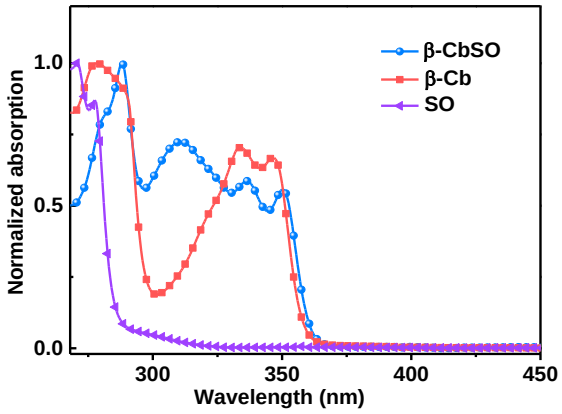

Figure S21. Normalized absorption spectra of **β-CbSO, β-Cb** and **SO** in dilute MeCN solution.

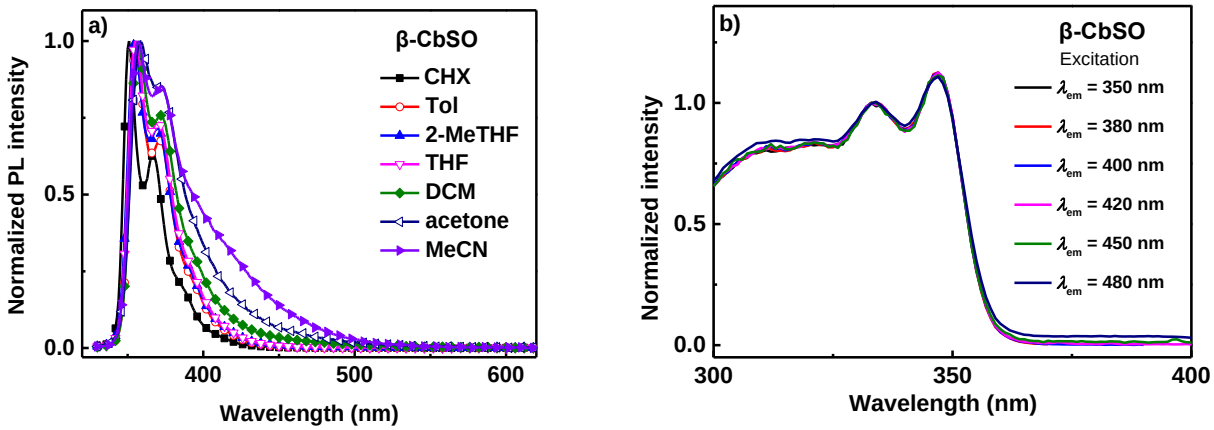

Figure S22. a) PL emission spectra of **β-CbSO** in solutions with different polarity environments under ambient conditions (λ_{ex} = 320 nm, 10^{-5} M). b) Excitation spectra of **β-CbSO** in dilute MeCN solution.

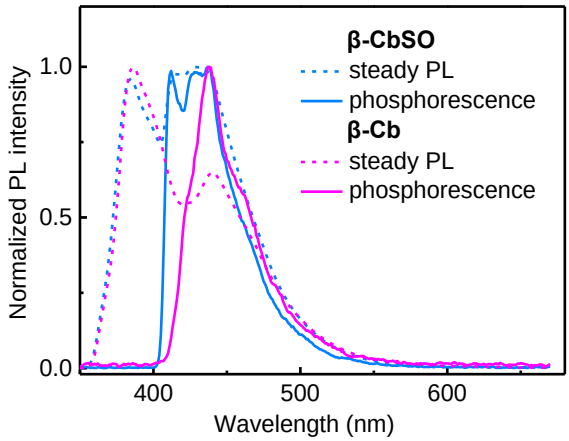

Figure S23. Steady-state PL and phosphorescence spectra (delay 40 Hz) of **β-CbSO** (blue line) and **β-Cb** (pink line) in dilute 2-MeTHF solution (10^{-5} M, λ_{ex} = 330 nm) at 77 K.

Accordingly, the triplet energy level of **β-CbSO** (E_{T1}) is determined to be 3.02 eV in 2-MeTHF solution.

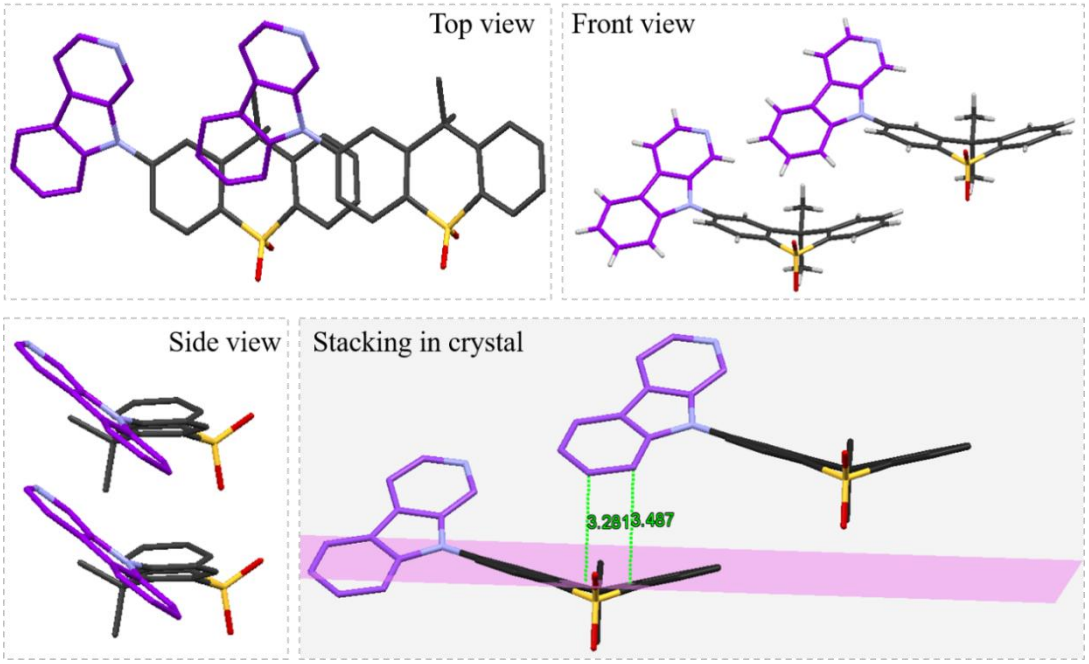

Figure S24. Molecular stacking in single crystal sample of **β-CbSO**. The shortest distance between the π systems of **β-Cb** and **SO** is 3.281 Å.

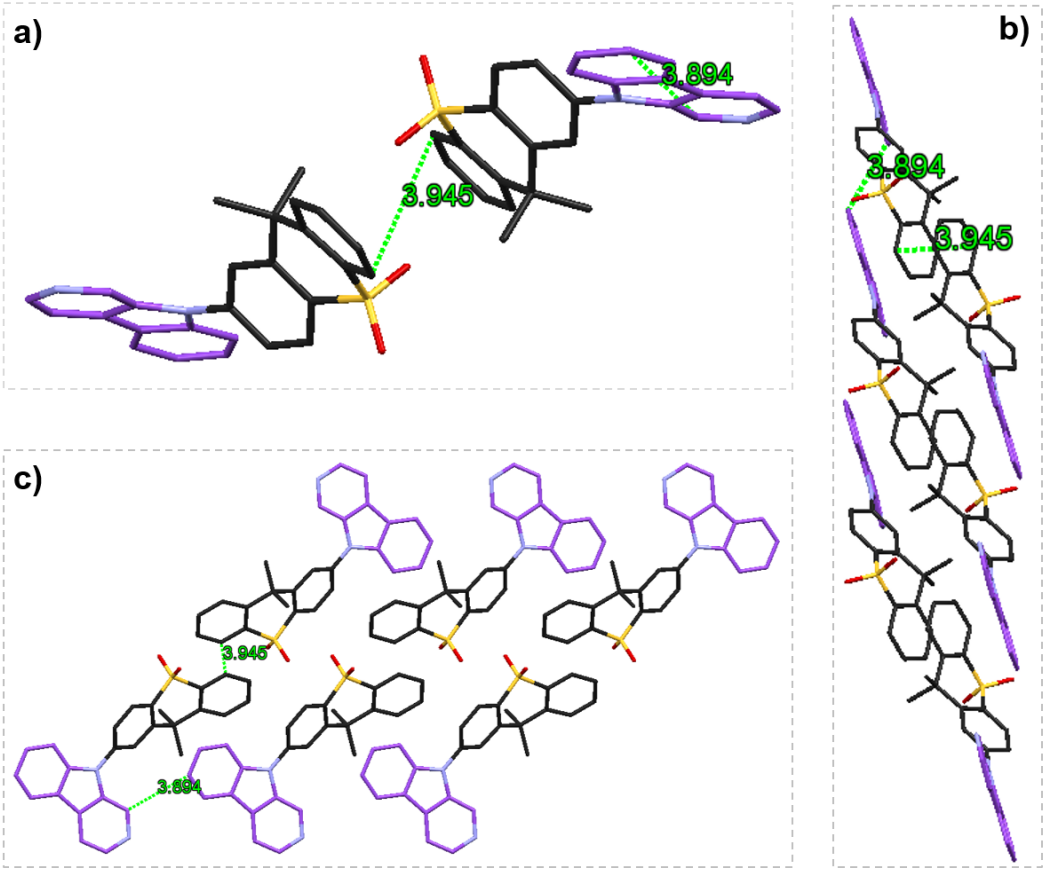

Figure S25. Molecular packing in the crystal lattice of **β-CbSO**. View down: a) the a-axis; b) the b-axis; and c) the c-axis, respectively.

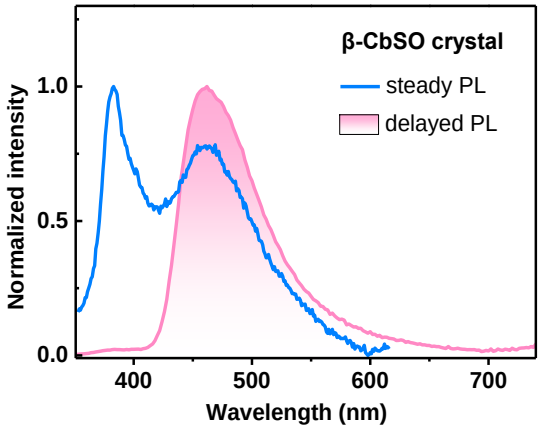

Figure S26. Steady state and delayed PL spectra (delay 0.1 ms) of crystalline **β-CbSO** (λ_{ex} = 330 nm).

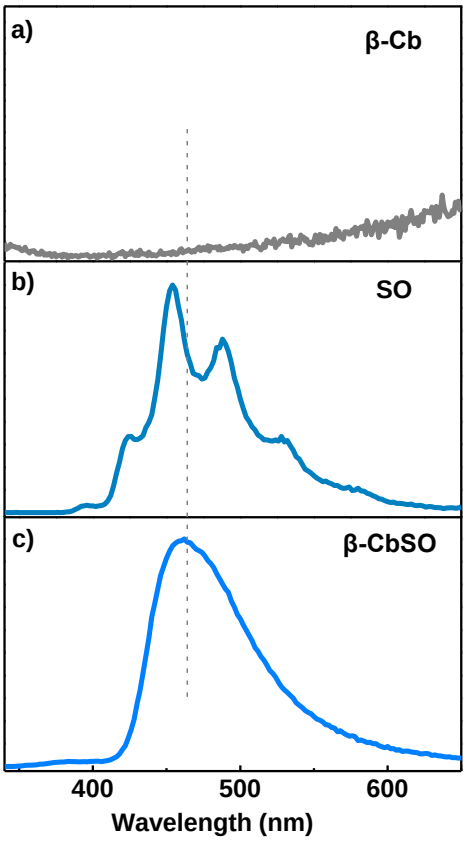

Figure S27. Delayed PL spectra (delay time = 0.1 ms) of: a) crystalline **β-Cb**; b) crystalline **SO**, and c) crystalline **β-CbSO** (λ_{ex} = 330 nm).

Because the delayed emission spectrum of the lower-energy UOL band of crystalline **β-CbSO** differs distinctly from that of either crystalline **β-Cb** or crystalline **SO** (Figure S27), the ultralong-lived emission band of crystalline **β-CbSO** should not originate from the RTP from either **β-Cb** or **SO**, but from the I-TSCT excited state of **β-Cb** ··**SO** [I-TSCT$_{(\beta\text{-Cb}\cdots\text{SO})}$*]. Consistent with **CzSO**, as I-TSCT complexes own very small energy differences between their singlet [S_1^*(I-TSCT)] and triplet [T_1^*(I-TSCT)] excited states due to their spatially separated electron and hole wavefunctions, it is difficult to differentiate their phosphorescence [radiative deactivation of their T_1^*(I-TSCT) excitons] from their ultralong TADF [radiative deactivation of their S_1^*(I-TSCT) excitons populated *via* RISC]. Therefore, the persistent luminescence of **β-CbSO** crystals can also be attributed to the ultra-long TADF and RTP dual-channel emission from its I-TSCT excitons.

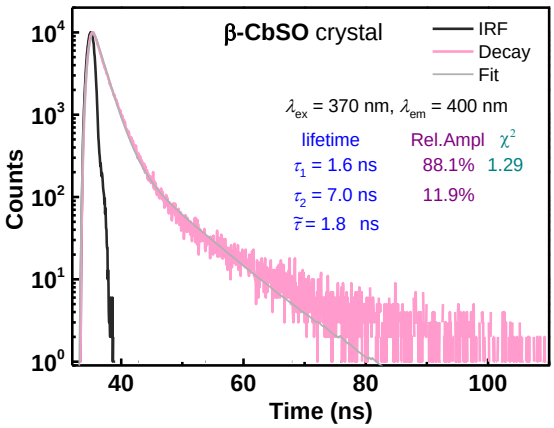

Figure S28. PL decay profile of the higher-energy PL emission band of crystalline **β-CbSO** recorded at λ_{em} = 400 nm under ambient conditions (λ_{ex} = 370 nm) with a time-range window of 200 ns.

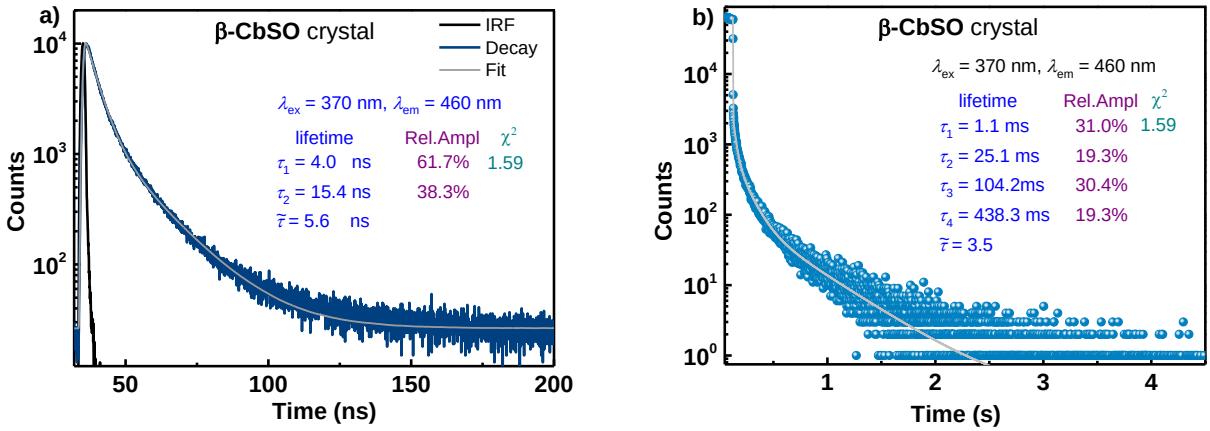

Figure S29. PL decay profiles of the lower-energy PL emission band of crystalline **β-CbSO** recorded at λ_{em} = 460 nm under ambient conditions (UV-light excitation, λ_{ex} = 370 nm) at different time-range windows of: a) 200 ns; and b) 5.6 s.

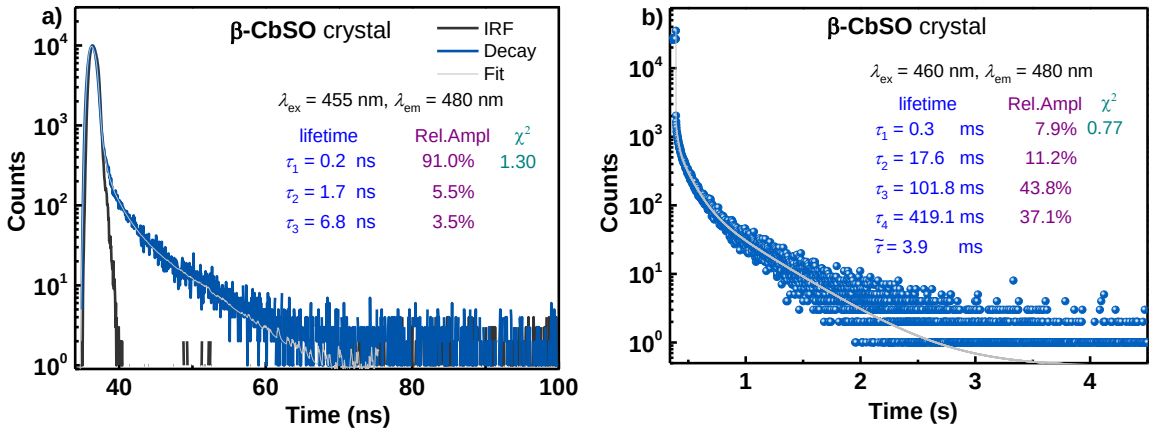

Figure S30. PL decay profiles of the lower-energy emission band of crystalline **β-CbSO** recorded at λ_{em} = 480 nm under ambient conditions (visible light excitation, λ_{ex} = 455 or 460 nm) at different time-range windows of: a) 200 ns; and b) 5.6 s.

After careful comparison between the PL decay and IRF curves, we conjectured that the species with the shortest lifetime (τ < 1 ns) in Figure S30a may originate from the excitation source (nano-diode 455 nm) through light scattering.

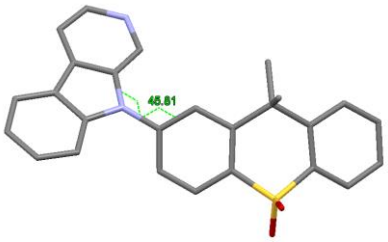

Figure S31. The molecular structure in **β-CbSO** single-crystals. The torsion angles between **β-Cb** and **SO** unit is indicated by green dashed lines: 45.81°.

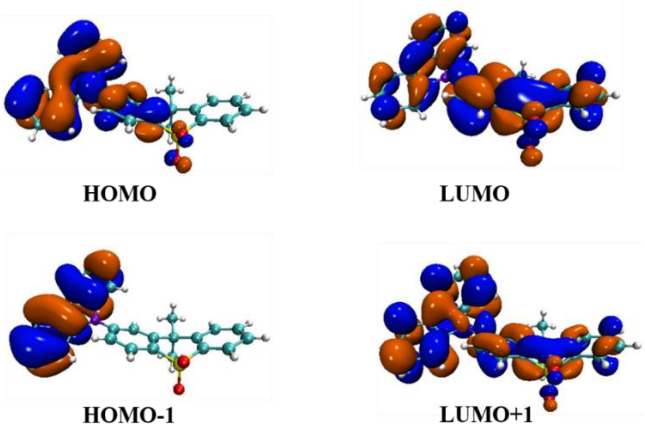

Figure S32. Calculated electron cloud distributions of HOMO, HOMO-1, LUMO and LUMO+1 orbitals of monomeric **β-CbSO** (isovalue is 0.02).

Table S7. The singlet and triplet excited state transition configurations of monomeric **β-CbSO** revealed by TD-DFT calculations (isovalue is 0.02).

monomeric **β-CbSO**					
	Transition configuration	CI	Transition Character	*f*	Δ*E*
S_0-S_1		60.9%	intramolecular CT + $LE_{(β\text{-}Cb)}$	0.210	3.996 eV
S_0-S_2		60.4%	intramolecularCT + $LE_{(β\text{-}Cb)}$	0.1733	4.081 eV
S_0-S_3		90.2%	intramolecular CT	0.0037	4.404 eV
S_0-S_4		65.6%	intramolecular CT	0.0019	4.645 eV
S_0-S_5		74.1%	intramolecular CT + $LE_{(β\text{-}Cb)}$	0.0569	4.736 eV
S_0-S_6	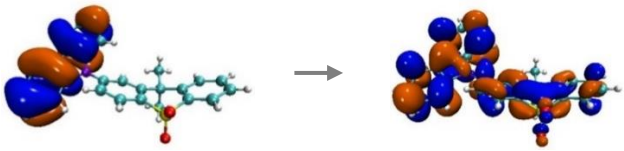	66.9%	intramolecular CT + $LE_{(β\text{-}Cb)}$	0.0407	4.760 eV
S_0-T_1		36.7%	intramolecular CT + $LE_{(β\text{-}Cb)}$	0.000	3.168 eV
S_0-T_2		49.5%	intramolecular CT + $LE_{(β\text{-}Cb)}$	0.000	3.254 eV
S_0-T_3	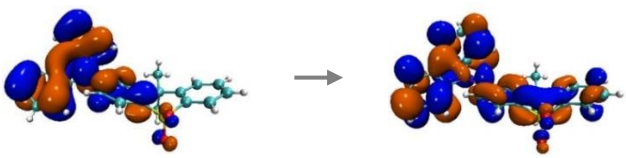	61.9%	intramolecular CT + $LE_{(β\text{-}Cb)}$	0.000	3.282 eV

Table S8. The singlet and triplet excited state transition configurations of monomeric **β-CbSO** revealed by TD-DFT calculations. The matched triplet excited states that contain the same orbital transition components of S_1 were highlighted in red.

	n-th	Energy (eV)	Transition configuration (%)
S_n	1	3.996	H→L (60.9)
T_n	1	3.168	H-5→L+1 (3.9), H-1→L+1 (36.7), H→L (3.0), H→L+5 (10.0)
	2	3.254	H-6→L (8.6), H-6→L+1 (2.5), H→L (49.6), H→L+1 (3.0)
	3	3.282	H-5→L +5(2.8), H-1→L +1(8.3), H→L +1(61.9), H→L +5(3.2)
	4	3.570	H-4→L (7.5), H-4→L+1 (2.8), H-4→L+2 (5.4), H-4→L+3 (6.5), H-3→L (6.3), H-3→L+1 (3.0), H-3→L+3 (22.8), H-3→L+4 (7.0)
	5	3.970	H-2→L+1 (44.3), H-2→L+6 (4.2), H-2→L+7 (5.3), H→L+6 (3.6)
	6	3.974	H-9→L+1 (1.8), H-7→L+2 (14.9), H-7→L+4 (2.2), H-5→L+5 (5.5), H-2→L+1 (13.3), H-2→L+6 (1.7), H-2→L+7 (1.7), H-1→L+7 (2.0), H→L (14.0)
	7	4.049	H-6→L+2 (5.3), H-5→L+1 (1.7), H→L+2 (70.0), H→L+4 (5.4), H→L+5 (2.3), H→L+6 (1.7)
	8	4.123	H-5→L+1 (17.6), H-1→L (5.8), H→L+5 (41.2), H→L+7 (1.8)

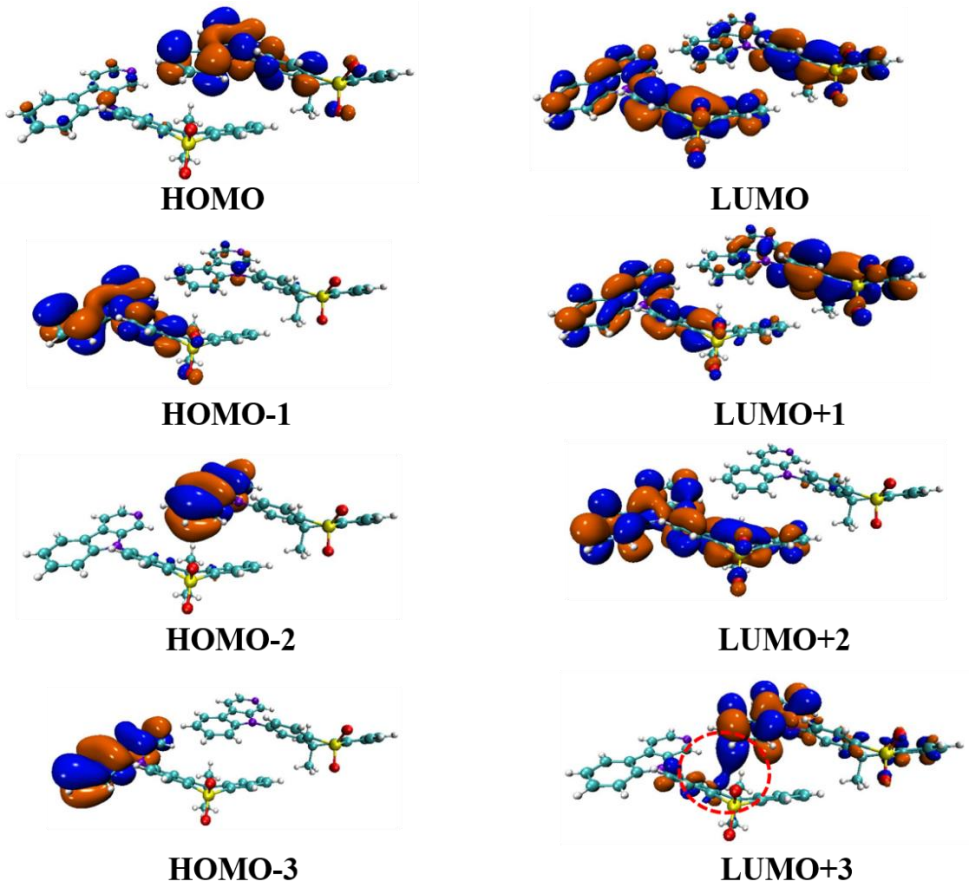

Figure S33. Calculated electron cloud distribution of HOMO, HOMO-1, HOMO-2, HOMO-3, LUMO, LUMO+1, LUMO+2 and LUMO+3 orbitals of dimeric **β-CbSO** aggregates (isovalue is 0.02).

Table S9. The singlet and triplet excited state transition configurations of dimeric **β-CbSO** aggregates revealed by TD-DFT calculations (isovalue is 0.02).

dimeric **β-CbSO**					
	Transition configuration	CI	Transition Character	*f*	Δ*E*
S_0-S_1	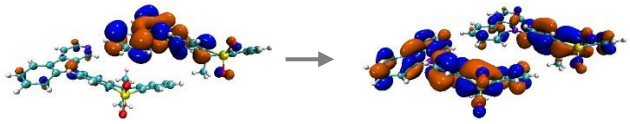	48.8%	intramolecular CT + **intermolecular CT**	0.375	3.952 eV
S_0-S_2	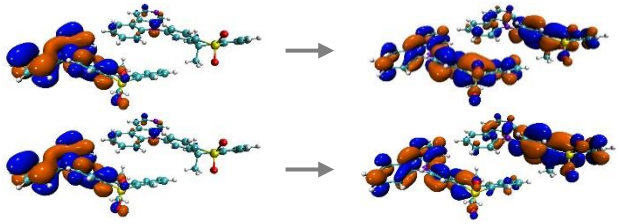	40.0% 24.1%	intramolecular CT + **intermolecular CT**	0.151	3.985 eV
S_0-S_3	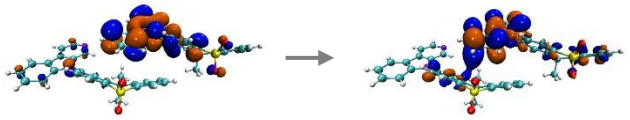	75.9%	**intermolecular CT** + $LE_{(β\text{-}Cb)}$	0.022	4.042 eV
S_0-S_4	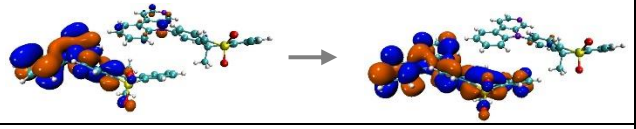	51.2%	**intramolecular CT** + $LE_{(β\text{-}Cb)}$	0.125	4.071 eV
S_0-S_5	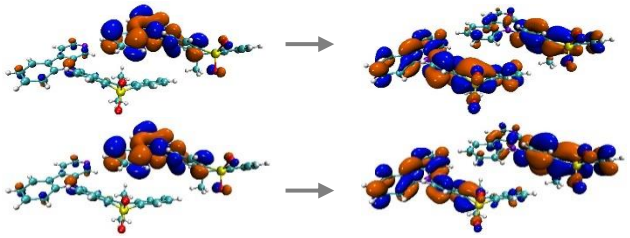	29.6% 28.9%	intramolecular CT + **intermolecular CT**	0.047	4.146 eV
S_0-S_6	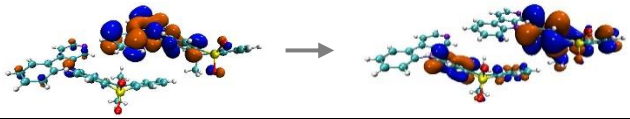	66.0%	intramolecular CT + **intermolecular CT**	0.002	4.320 eV

Table S10. The singlet and triplet excited state transition configurations of dimeric **β-CbSO** aggregates revealed by TD-DFT calculations. The matched triplet excited states that contain the same orbital transition components of S_1 were highlighted in red.

	n-th	Energy (eV)	Transition configuration (%)
S_n	1	3.952	H→L (48.8)
T_n	1	3.165	H-11→L+2 (3.2), H-3→L (13.4), H-3→L+1 (4.1), H-3→L+2 (28.0), H-3→L+3 (0.1)
	2	3.165	H-18→L+15 (2.0), H-8→L+3 (1.6), H-2→L+1 (3.9), H-2→L+3 (49.1)
	3	3.231	H-14→L+4 (2.3), H-1→L+1 (2.3), H→L+1 (28.5), H→L+6 (6.7)
	4	3.249	H-13→L (2.6), H-12→L (2.9), H-12→L+1 (1.7), H-1→L (28.9), H-1→L+1 (12.1)
	5	3.279	H-11→L+2 (1.7), H-3→L (3.6), H-3→L+1 (3.7), H-3→L+2 (6.9), H-1→L (6.4), H-1→L+1 (9.8), H-1→L+2 (48.7)
	6	3.296	H-2→L+3 (8.0), H-1→L+3 (3.6), H→L+3 (66.9)
	7	3.569	H-13→L+8 (2.9), H-10→L (1.7), H-10→L+4 (4.2), H-10→L+6 (1.9), H-10→L+7 (1.7), H-10→L+8 (20.5), H-9→L+1 (5.5), H-8→L+1 (2.0)
	8	3.570	H-9→L+9 (3.2), H-7→L+2 (5.5), H-7→L+9 (6.1)
	9	3.943	H-18→L+3 (2.0), H-14→L+4 (4.5), H-13→L+1 (2.0), H-9→L+11 (1.5), H-2→L+15 (1.6), H→L (6.8), H→L+4 (10.2)
	10	3.963	H-12→L (1.5), H-12→L+5 (3.2), H-3→L+14 (2.2), H-1→L+2 (2.1), H-1→L+5 (1.4), H-1→L+7 (1.8), H→L (1.6)
	11	3.978	H-4→L+1 (4.3), H-4→L+3 (69.9), H-4→L+13 (5.5), H-4→L+15 (6.4)
	12	3.990	H-5→L (7.4), H-5→L+1 (7.8), H-5→L+2 (18.0), H-5→L+12 (2.4), H-5→L+14 (2.4), H→L+4 (30.0), H→L+13 (1.9)
	13	3.992	H-5→L (9.9), H-5→L+1 (10.9), H-5→L+2 (24.8), H-5→L+12 (3.3), H-5→L+14 (3.3), H→L (1.7), H→L+5 (1.7), H→L+8 (1.8)
	14	4.034	H-13→L+5 (1.8), H-12→L+5 (2.8), H-1→L+3 (9.1), H-1→L+4 (6.8), H-1→L+5 (49.8), H-1→L+12 (1.6), H→L (0.03)
	15	4.118	H-11→L+12 (2.3), H-3→L (4.2), H-3→L+1 (4.8), H-3→L+2 (13.7), H-1→L+10 (38.2), H→L (0.8)
	16	4.123	H-9→L+3 (3.9), H-6→L+3 (2.8), H-2→L+3 (16.5), H-1→L+11 (1.6), H→L (7.7), H→L+1 (4.7), H→L+4 (2.5), H→L+11 (32.2)
	17	4.148	H-8→L+3 (1.9), H-1→L (3.1), H→L (34.0), H→L+1 (18.9), H→L+4 (1.4), H→L+7 (1.6)
	18	4.289	H-14→L+4 (3.1), H-8→L+11 (2.6), H-1→L+12 (1.7), H→L (1.7), H→L+3 (4.7), H→L+6 (1.4), H→L+13 (14.7)

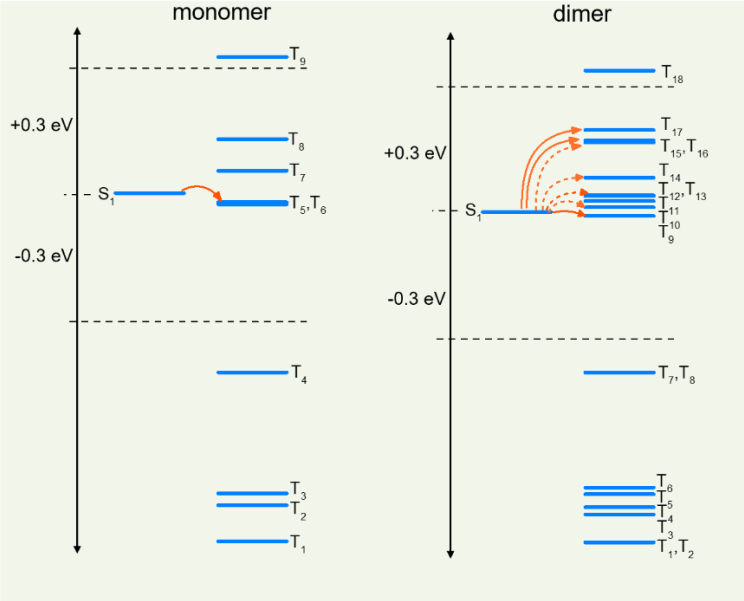

Figure S34. The calculated energy levels of monomeric and dimeric **β-CbSO** aggregates based on PBE0/6-311g (d) calculations.

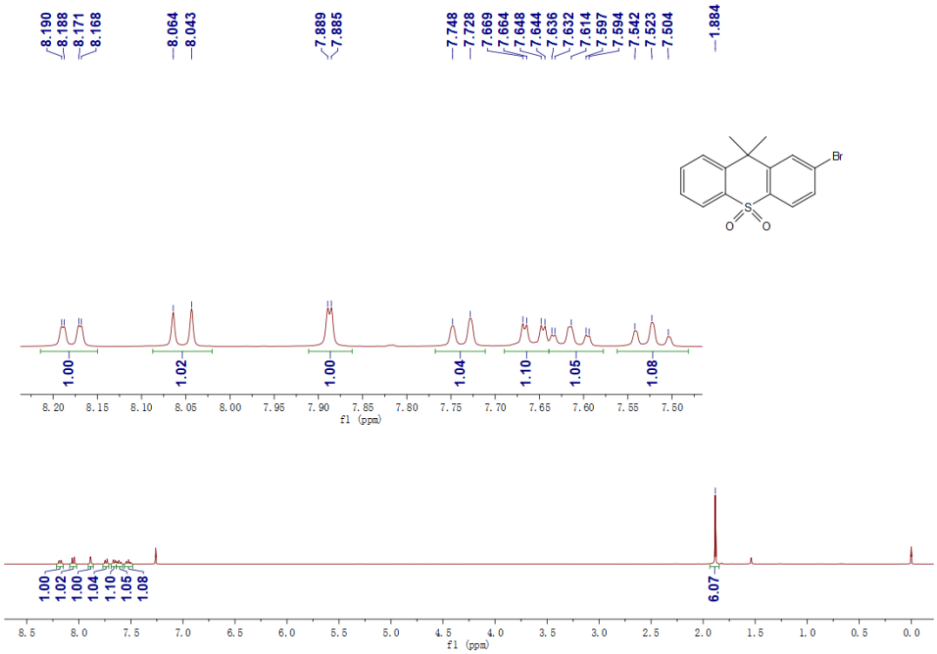

Figure S35. The ^{1}H NMR spectrum of the intermediate **3** in $CDCl_3$.

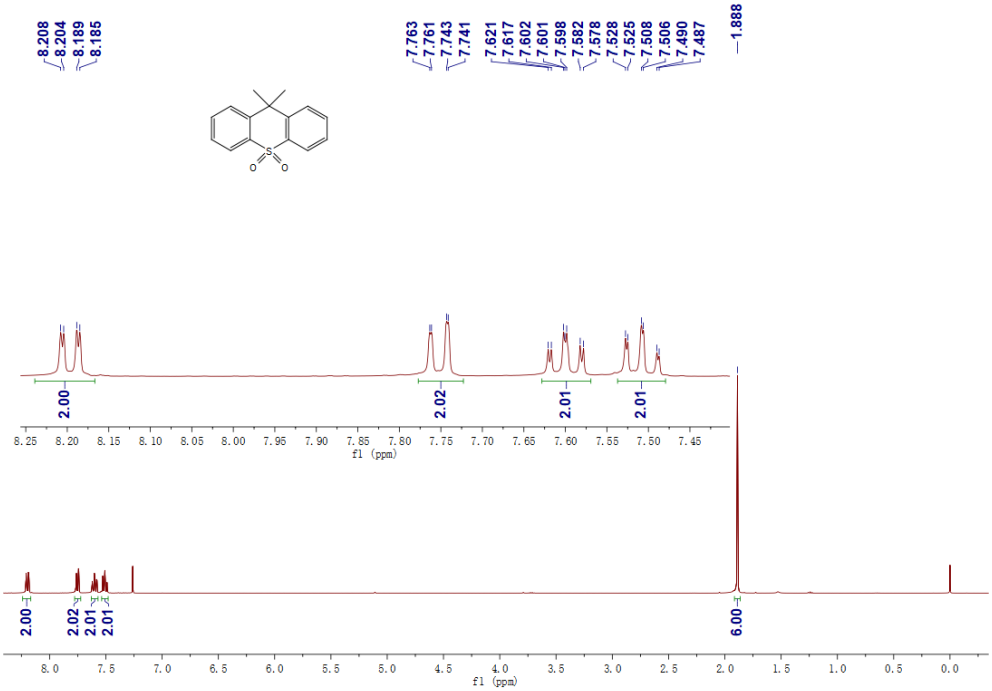

Figure S36. The ^{1}H NMR spectrum of **SO** in $CDCl_3$.

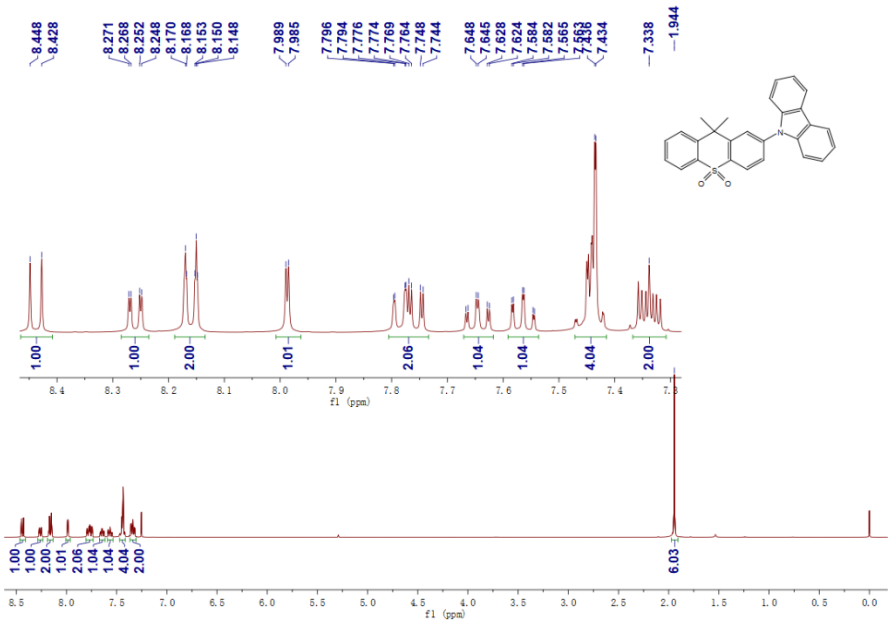

Figure S37. The ^{1}H NMR spectrum of **CzSO** in $CDCl_3$.

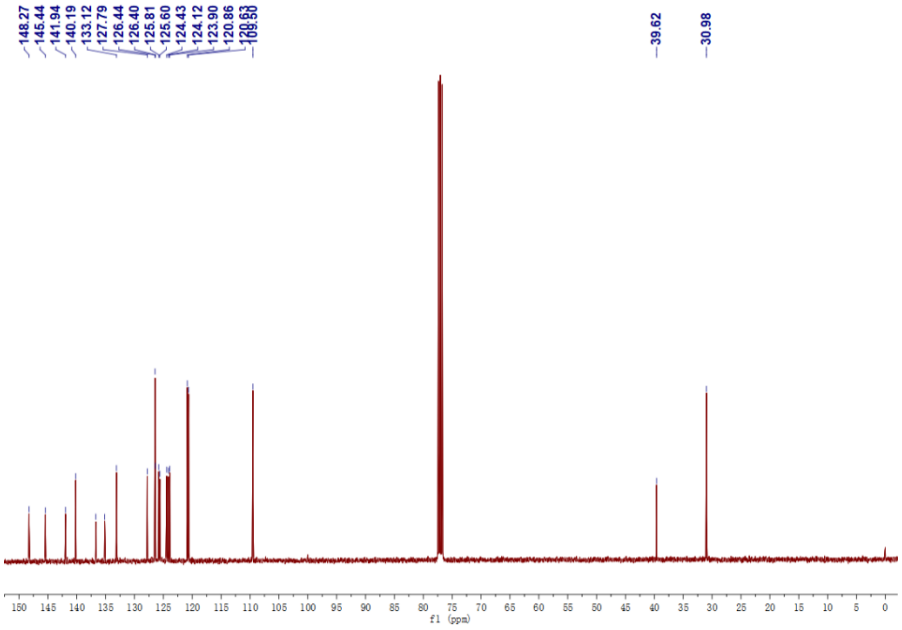

Figure S38. The ^{13}C NMR spectrum of **CzSO** in $CDCl_3$.

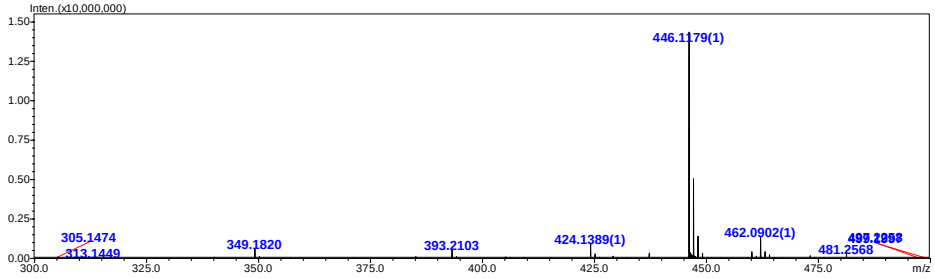

Figure S39. High resolution ESI mass spectrum of **CzSO**. Calcd for $C_{27}H_{21}NO_2SNa^+$ $[M+Na]^+$ 446.1185, found 446.1179.

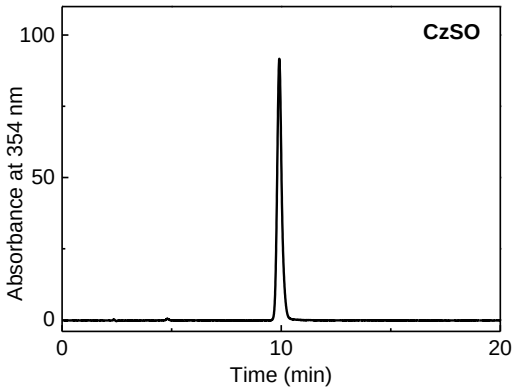

Figure S40. HPLC characterization result of **CzSO** (eluent: acetonitrile/water (70/30), monitored at 354 nm).

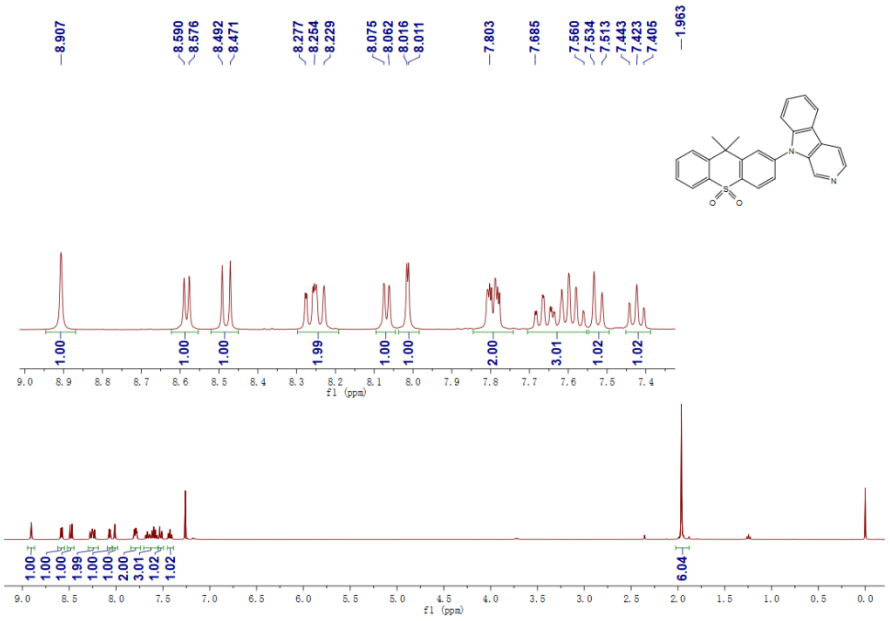

Figure S41. The ^{1}H NMR spectrum of **β-CbSO** in $CDCl_3$.

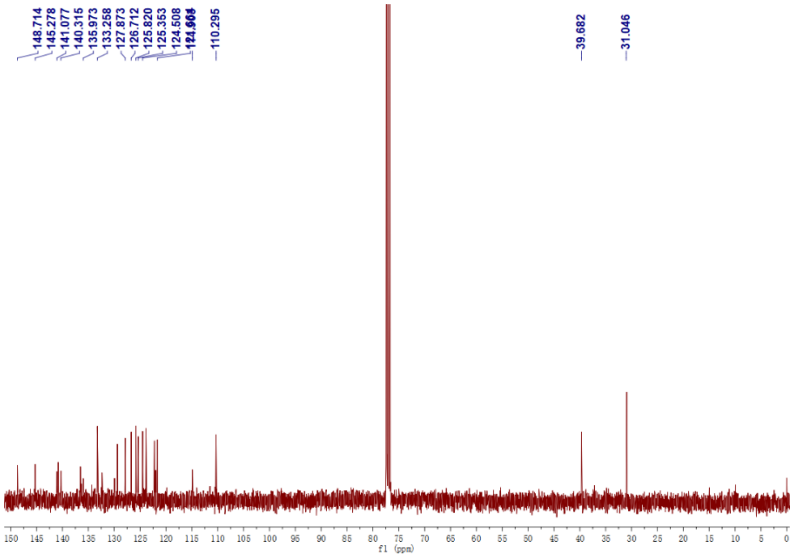

Figure S42. The ^{13}C NMR spectrum of **β-CbSO** in $CDCl_3$.

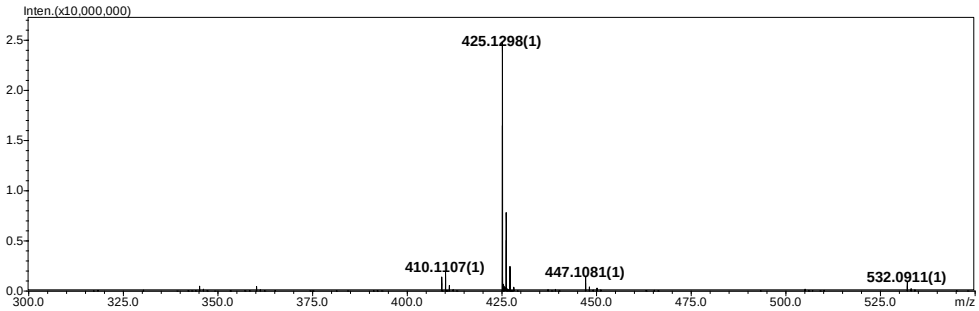

Figure S43. High resolution ESI mass spectrum of **β-CbSO**. Calcd for $C_{26}H_{20}N_2O_2SH^+$ $[M+H]^+$ 425.1318, found 425.1298.

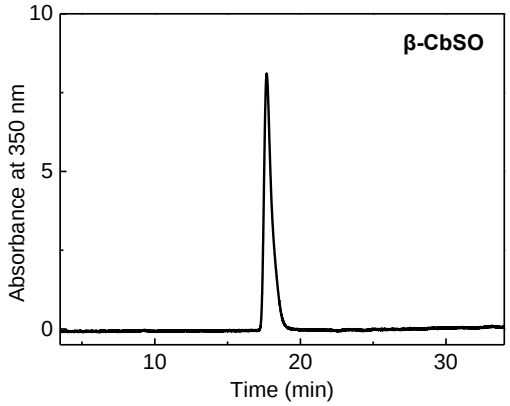

Figure S44. HPLC characterization result of **β-CbSO** (eluent: methanol/water (67/33), monitored at 350 nm).

3) A survey of reported ultralong organic luminescence (UOL) materials

Table S11. Molecular structures, excitation wavelength, lifetime, efficiency, emission wavelength and emission assignment of the pure organic long persistent luminescence materials with a lifetime over 100 ms under ambient conditions.

Compound	Molecular structure	λ_{ex}	τ_{uol}	ϕ_{uol}	$\lambda_{uol,max}$	Emission assignment	Ref.
CzSO	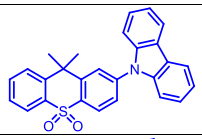	440 nm	453 ms	26.3%	490 nm	Intermolecular through- space CT between Cz and SO unit	This work
β-CbSO	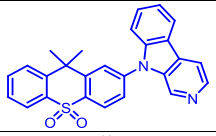	440 nm	419	4.4%	460 nm	Intermolecular through space CT between β-Cb and SO unit	This work
Cz	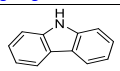	365 nm	910 or 470 ms	-	555 nm	Cz aggregates	[2] [3]
C1	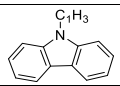	365 nm	220 ms	-	~550 nm	Cz aggregates	[4]
C3	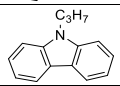	365 nm	810 ms	-	~550 nm	Cz aggregates	[4]
C4	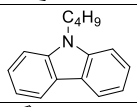	365 nm	490 ms	-	~560 nm	Cz aggregates	[4]
CC2Br	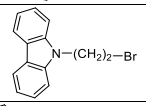	365 nm	160 ms	1.6%	~550 nm	Cz aggregates	[3]
CC4PhBr	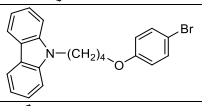	365 nm	340 ms	9.5%	~555 nm	Cz aggregates	[3]
CC5PhBr	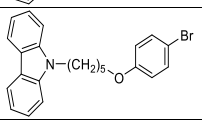	365 nm	197 ms	2.8%	~555 nm	Cz aggregates	[3]
CC6PhBr	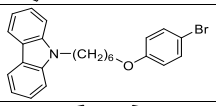	365 nm	200 ms	39.5%	~555 nm	Cz aggregates	[3]
CZEO	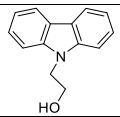	364 nm	740 ms	-	551 nm	Cz aggregates	[5]
C-C4-Br	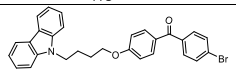	365 nm	140 ms	11%	570/620 nm	Cz aggregates	[6]
*p*BrPhCz	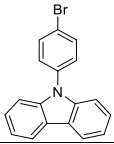	400 nm	250ms	9.5%	550/598 nm	Cz aggregates	[7]
*m*BrPhCz	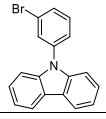	400 nm	240 ms	6.6%	548/598 nm	Cz aggregates	[7]

PhCz	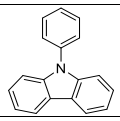	400 nm	270 ms	1.8%	548/596 nm	Cz aggregates	[7]
pCNPhCz	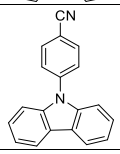	365 nm or 405nm	920 ms	1.8%	545/594 nm	Cz aggregates	[8]
mCNPhCz	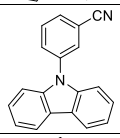	365 nm	810 ms	3.7%	548/599 nm	Cz aggregates	[8]
oCNPhCz	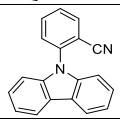	365 nm	650 ms	2.9%	543/593 nm	Cz aggregates	[8]
DCNPhCz	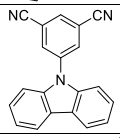	365 nm	480 ms	8.6%	544/593 nm	Cz aggregates	[8]
PDCz	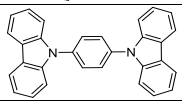	365 nm	560 ms	2.5%	558 nm	Cz aggregates	[9]
PDBCz	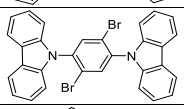	365 nm	217 ms	38.1%	546 nm	Cz aggregates	[9]
CZ-DBF	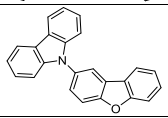	365 nm	650 ms	14.3%	550 nm	Cz aggregates	[10]
CZ-DBFBr	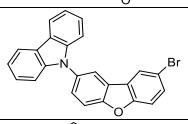	365 nm	540 ms	41.2%	550 nm	Cz aggregates	[10]
CZ-DBT	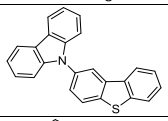	365 nm	450 ms	10.1%	550 nm	Cz aggregates	[10]
CZ-DBTBr	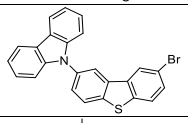	365 nm	420 ms	12.1%	550 nm	Cz aggregates	[10]
DCzCT	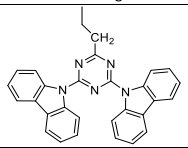	365 nm	651 ms	9.7%	546 nm	Cz aggregates	[11]
DCzOT	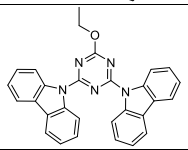	365 nm	789 ms	9.2%	543 nm	Cz aggregates	[11]
DCzNT	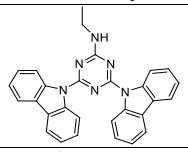	365 nm	633 ms	15.4%	553 nm	Cz aggregates	[11]
DECzT	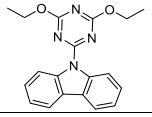	365 nm	1350 ms	0.6%	529/574 nm	Cz aggregates	[12]

DPhCzT	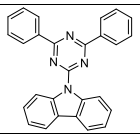	365 nm	1060 ms	1.25%	530/575 nm	Cz aggregates	[12]
CzDClT	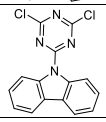	365 nm	490 ms	2.1%	543/591 nm	Cz aggregates	[12]
p-BrTCz	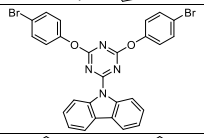	365 nm	155 ms	7.7%	539/581/634 nm	Cz aggregates	[13]
m-BrTCz	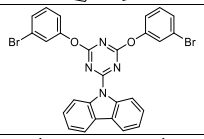	365 nm	109 ms	13%	530/572/622 nm	Cz aggregates	[13]
o-BrTCz	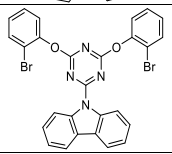	365 nm	156 ms	2.3%	532/573/624 nm	Cz aggregates	[13]
MCzT	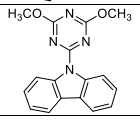	365 nm	1131 ms	2.5%	538/572 nm	Cz aggregates	[14]
ECzT	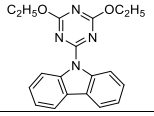	365 nm	1281 ms	-	537/570 nm	Cz aggregates	[14]
PCzT	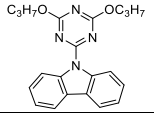	365 nm	146 ms	1.8%	528/570 nm	Cz aggregates	[14]
BCzT	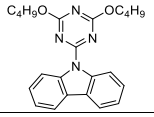	365 nm	102 ms	1.1%	530/570 nm	Cz aggregates	[14]
FCzT	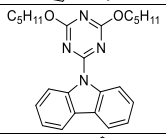	365 nm	1228 ms	0.8%	526/573 nm	Cz aggregates	[14]
SPCzT	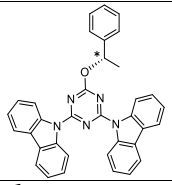	365 nm	420 ms	0.58%	539/580 nm	Cz aggregates	[15]
MTOD	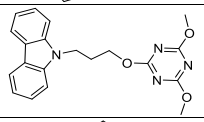	365 nm	861 ms	-	556 nm	Cz aggregates	[16]
DNCzP	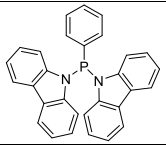	365 nm	230 ms	0.08%	587/644 nm	Cz aggregates	[17]
DNCzPO	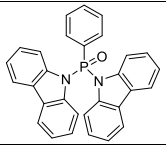	365 nm	670 ms	2.8%	537/582/634 nm	Cz aggregates	[17]

DNCzPS	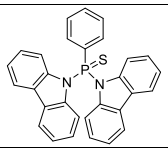	365 nm	510 ms	4.0%	530/577/627 nm	Cz aggregates	[17]
PhCz	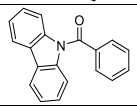	376 nm	646 ms	0.7%	530/570 nm	Cz aggregates	[18]
CPhCz	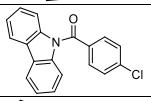	410 nm	847 ms	8.3%	530/570 nm	Cz aggregates	[18]
BPhCz	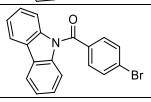	388 nm	667 ms	3.4%	530/570 nm	Cz aggregates	[18]
24CPhCz	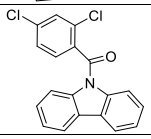	365 nm	1058 ms	2.5%	532/574 nm	Cz aggregates	[19]
34CPhCz	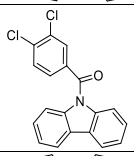	365 nm	770 ms	3.4%	537/582/636 nm	Cz aggregates	[19]
DCED	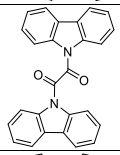	365 nm	296 ms	3.5%	529/572/623 nm	Cz aggregates	[20]
o-PBCM	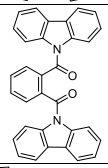	365 nm	344 ms	10.2%	529/572/623 nm	Cz aggregates	[20]
m-PBCM	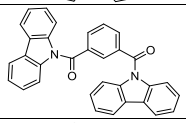	365 nm	711 ms	5.7%	529/572/623 nm	Cz aggregates	[20]
p-PBCM	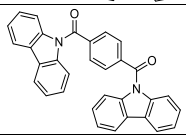	365 nm	312 ms	9.8%	529/572/623 nm	Cz aggregates	[20]
BCz-BP	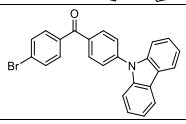	365 nm	280 ms	5.0%	549/602 nm	Cz aggregates	[21]
CZBP 2015.9 tang	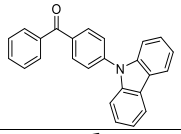	365 nm	518 ms	1.40%	552/569/597 nm	Cz aggregates	[22]
o-Cz	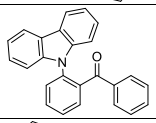	UV and visible light	840 ms	16.6%	472 nm/ 542 nm	Emission from intramolecular through-space charge-transfer and Cz aggregates	[23]
CPM	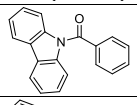	365 nm	748 ms	3.17%	530 nm	Cz aggregates	[24]
CMPM	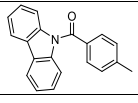	365 nm	340 ms	1.98%	530 nm	Cz aggregates	[24]

CMOPM	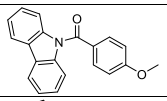	365 nm	114 ms	0.51%	550 nm	Cz aggregates	[24]
CBA	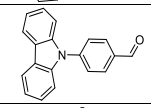	360 nm	540 ms	-	550 nm	Cz aggregates	[25]
1CA	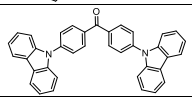	350 nm	373 ms	-	553/600 nm	Cz aggregates	[26]
p-1	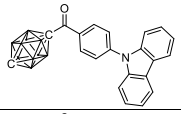	UV and visible light	153 ms	7.1%	569 nm	Cz aggregates	[27]
m-1	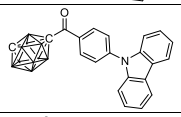	UV and visible light	134 ms	0.9%	565 nm	Cz aggregates	[27]
p-2	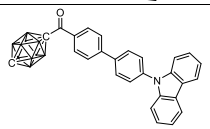	UV and visible light	666 ms	2%	553 nm	Cz aggregates	[27]
m-2	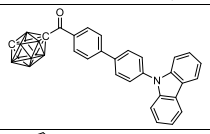	UV and visible light	385 ms	4%	547 nm	Cz aggregates	[27]
DME	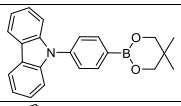	365 nm	430 ms	-	545 nm	Cz aggregates	[28]
PE	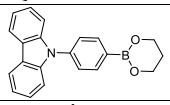	365 nm	264 ms	-	553 nm	Cz aggregates	[28]
o-MCBA	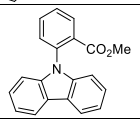	365 nm	619 ms	2.0%	550/600 nm	Cz aggregates	[29]
m-MCBA	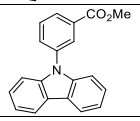	365 nm	795 ms	2.1%	545/595 nm	Cz aggregates	[29]
p-MCBA	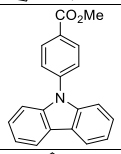	365 nm	129 ms	1.2%	560/590 nm	Cz aggregates	[29]
2-BACZ	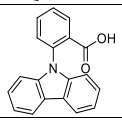	365 nm	568 ms	2.6%	558/599 nm	Cz aggregates	[30]
3-BACZ	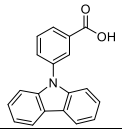	365 nm	602 ms	3.4%	546/592 nm	Cz aggregates	[30]
4-BACZ	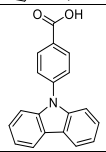	365 nm	558 ms	6.9%	549/594 nm	Cz aggregates	[30]
BCz-DPS	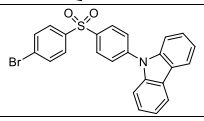	365 nm	120 ms	6.0%	558 nm	Cz aggregates	[21]

0M	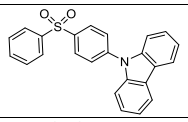	365 nm	360 ms	1.5%	565 nm	Cz aggregates	[31]
1M	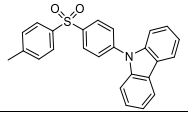	365 nm	820 ms	2.6%	546 nm	Cz aggregates	[31]
3M	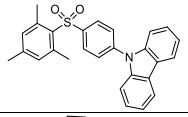	365 nm	830 ms	1.1%	542 nm	Cz aggregates	[31]
CzDPS	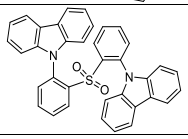	UV	465 ms	0.2%	565 nm	Cz aggregates	[32]
OMe-SPhT	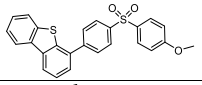	365 nm	171 ms	4.7%	563 nm	PhT	[33]
DOPPMO	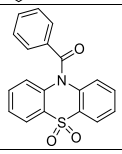	365 nm	455 ms	3.6%	488 nm	-	[34]
PEO	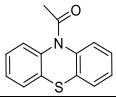	365 nm	238 ms	8.1%	521 nm	-	[34]
DOPEO	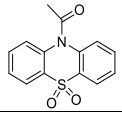	365 nm	876 ms	8.2%	514 nm	-	[34]
CS-H	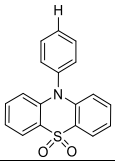	365 nm	188 ms	-	525 nm	-	[35]
CS-Br	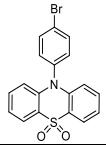	365 nm	268 ms	-	525 nm	-	[35]
CS-Cl	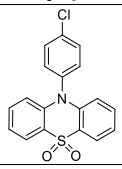	365 nm	256 ms	-	500 nm	-	[35]
CS-F	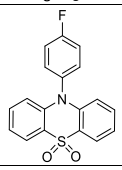	365 nm	410 ms	-	483/513 nm	-	[35]
CS-CF3	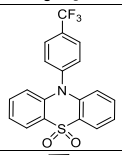	365 nm	299 ms	-	480/510 nm	-	[35]
CS-CH3	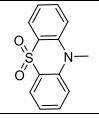	365 nm	245 ms	-	~520 nm	Stacking of phenothiazine 5,5-dioxide groups	[36]

CS-C3H7	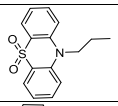	365 nm	327 ms	-	~520 nm	Stacking of phenothiazine 5,5-dioxide groups	[36]
CS-C4H9	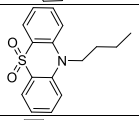	365 nm	181 ms	-	~520 nm	Stacking of phenothiazine 5,5-dioxide groups	[36]
CS-C5H11	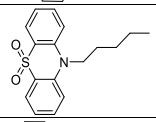	365 nm	205 ms	-	~520 nm	Stacking of phenothiazine 5,5-dioxide groups	[36]
CzS-CN		365 nm	226 ms	-	521 nm	-	[37]
Id	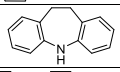	365 nm	402 ms	-	525 nm	H-aggregation	[2]
DEOPh	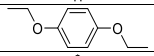	254 nm	710 ms	0.3%	515/547 nm	H-aggregation	[12]
IPA	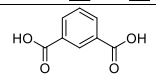	340-400 nm	290 ms	-	494 nm	-	[38]
24FPB	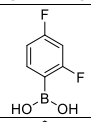	365 nm	2500 ms	2.4%	515 nm	H-aggregation	[39]
2FPB		365 nm	920 ms	1.0%	482 nm	-	[39]
234FPB	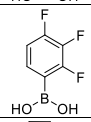	365 nm	490 ms	0.2%	470 nm	-	[39]
PBA-MeO		295 nm	2240 ms	-	483 nm	effective π–π stacking	[40]
PBA-F	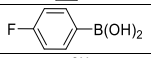	280 nm	1340 ms	-	492 nm		[40]
tPBA-MeO	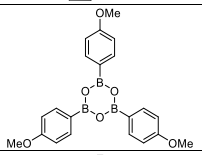	301 nm	710 ms	-	503 nm	-	[40]
tPBA-F	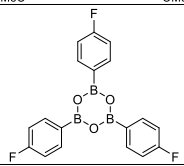	280 nm	1960 ms	-	500 nm	-	[40]
PDBEG	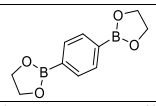	254 nm	1600 ms	-	503 nm	-	[41]
1	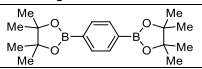	254 nm	1850 ms	2%	460/500 nm	-	[42]
TPB[a)]	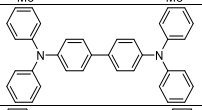	365 nm	700 ms	4.6%	521 nm	-	[43]
BipyDpa [a)]	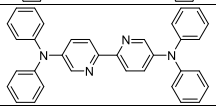	365 nm	176 ms	<1%	542 nm	-	[43]
PhenDpa [a)]	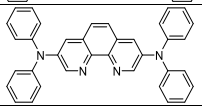	365 nm	330 ms	5.7%	516 nm	-	[43]

PhenTpa [a)]	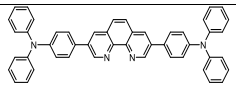	365 nm	680 ms	1.2%	544 nm	-	[43]
8	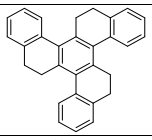	340 nm	380 ms	5.6%	566 nm	the non-planar configuration allows for pronounced SOC and a high triplet energy	[44]
PNA [b)]	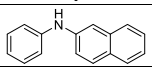	365 nm	173 ms	17%	508/546/589 nm	guest-host doping	[45]
AN-MA	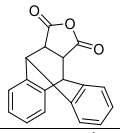	365 nm	1584 ms	-	490 nm	Intramolecular through-space conjugation	[46]
a	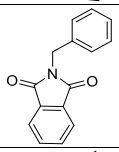	365 nm	243 ms	0.8%	553 nm	minimizes intermolecular interactions to reduce non-radiative decay pathways in the solid state.	[47]
b	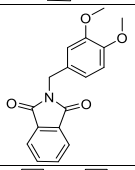	365 nm	371 ms	3.5%	548 nm	minimizes intermolecular interactions to reduce non-radiative decay pathways in the solid state.	[47]
PBC [c)]	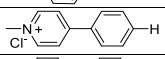	366 nm	2620 ms	9.7%	510 nm	host–guest complexation	[48]
PCC [c)]	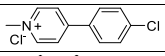	370 nm	275 ms	26.7%	500 nm	host–guest complexation	[48]
(R) –DMBDA [d)]	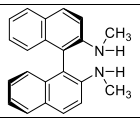	360 nm	670 ms	2.3%	560 nm	-	[49]
1	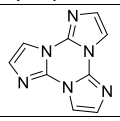	350 nm	990 ms	-	525 nm	H-aggregation	[50]
POP	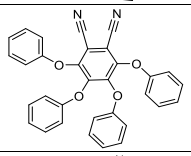	365 nm	253 ms	5.6%	520 nm	-	[51]
TOP	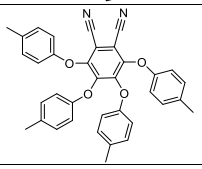	365 nm	248 ms	0.5%	473 nm	-	[51]
DMOT	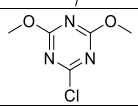	290 nm	2452 ms	7.2%	430 nm	H-aggregation	[52]
		340 nm	1638 ms		470 nm		
TMOT	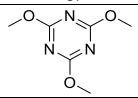	320 nm	582 ms	31.2%	465 nm	H-aggregation	[52]
		365 nm	745 ms		505 nm		
MOPT	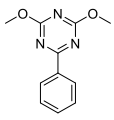	270 nm	137 ms	0.2%	370 nm	H-aggregation	[52]
		360 nm	544 ms		521 nm		
CYAD	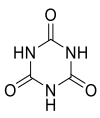	270 nm	453 ms	14.2%	380 nm	H-aggregation	[52]
		330 nm	552 ms		450 nm		

CAA	$CNCH_2COOH$	365 nm	862 ms	2.1%	506 nm	intermolecular interactions	[53]

[a] Doped in PMMA of 2 wt.%.(rigid matrix host–guest system); [b] Doped in DBBP; [c] Host–guest complexation, cucurbit [6]uril (CB[6]) as host; [d] Doped in β-estradiol (vide Scheme S2).

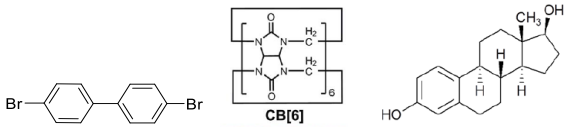

Scheme S2. Molecular structures of DBBP, CB[6] and β-estradiol.

4) References

[1] a) P. L. Santos, J. S. Ward, P. Data, A. S. Batsanov, M. R. Bryce, F. B. Dias, A. P. Monkman, *J. Mater. Chem. C* **2016**, *4*, 3815-3824; b) C. Fu, S. Luo, Z. Li, X. Ai, Z. Pang, C. Li, K. Chen, L. Zhou, F. Li, Y. Huang, Z. Lu, *Chem. Commun.* **2019**, *55*, 6317-6320.

[2] C. Sun, X. Ran, X. Wang, Z. Cheng, Q. Wu, S. Cai, L. Gu, N. Gan, H. Shi, Z. An, H. Shi, W. Huang, *J. Phys. Chem. Lett.* **2018**, *9*, 335-339.

[3] P. Xue, P. Wang, P. Chen, B. Yao, P. Gong, J. Sun, Z. Zhang, R. Lu, *Chem. Sci.* **2017**, *8*, 6060-6065.

[4] Z. Zhang, L. Tang, X. Fan, Y. Wang, K. Zhang, Q. Sun, H. Zhang, S. Xue, W. Yang, *J. Mater. Chem. C* **2018**, *6*, 8984-8989.

[5] Q. Huang, X. Mei, Z. Xie, D. Wu, S. Yang, W. Gong, Z. Chi, Z. Lin, Q. Ling, *J. Mater. Chem. C* **2019**, *7*, 2530-2534.

[6] S. M. A. Fateminia, Z. Mao, S. Xu, Z. Yang, Z. Chi, B. Liu, *Angew. Chem. Int. Ed.* **2017**, *56*, 12160-12164.

[7] J. Yuan, R. Chen, X. Tang, Y. Tao, S. Xu, L. Jin, C. Chen, X. Zhou, C. Zheng, W. Huang, *Chem. Sci.* **2019**, *10*, 5031-5038.

[8] J. Yuan, S. Wang, Y. Ji, R. Chen, Q. Zhu, Y. Wang, C. Zheng, Y. Tao, Q. Fan, W. Huang, *Mater. Horiz.* **2019**, *6*, 1259-1264.

[9] H. Shi, L. Song, H. Ma, C. Sun, K. Huang, A. Lv, W. Ye, H. Wang, S. Cai, W. Yao, Y. Zhang, R. Zheng, Z. An, W. Huang, *J. Phys. Chem. Lett.* **2019**, *10*, 595-600.

[10] W. Zhao, T. S. Cheung, N. Jiang, W. Huang, J. W. Y. Lam, X. Zhang, Z. He, B. Z. Tang, *Nat. Commun.* **2019**, *10*, 1595.

[11] L. Gu, H. Shi, C. Miao, Q. Wu, Z. Cheng, S. Cai, M. Gu, C. Ma, W. Yao, Y. Gao, Z. An, W. Huang, *J. Mater. Chem. C* **2018**, *6*, 226-233.

[12] Z. An, C. Zheng, Y. Tao, R. Chen, H. Shi, T. Chen, Z. Wang, H. Li, R. Deng, X. Liu, W. Huang, *Nat. Mater.* **2015**, *14*, 685-690.

[13] S. Cai, H. Shi, D. Tian, H. Ma, Z. Cheng, Q. Wu, M. Gu, L. Huang, Z. An, Q. Peng, W. Huang, *Adv. Funct. Mater.* **2018**, *28*.

[14] L. Gu, H. Shi, M. Gu, K. Ling, H. Ma, S. Cai, L. Song, C. Ma, H. Li, G. Xing, X. Hang, J. Li, Y. Gao, W. Yao, Z. Shuai, Z. An, X. Liu, W. Huang, *Angew. Chem. Int. Ed.* **2018**, *57*, 8425-8431.

[15] C. Ma, H. Ma, K. Ling, R. Zheng, M. Gu, L. Song, Z. An, H. Shi, W. Huang, *J. Mater. Chem. C* **2018**, *6*, 10179-10183.

[16] Z. Niu, C. Ma, W. Ye, H. Wang, W. Jia, H. Shi, H. Shi, Z. An, W. Huang, *RSC Adv.* **2019**, *9*, 19075-19078.

[17] Y. Tao, R. Chen, H. Li, J. Yuan, Y. Wan, H. Jiang, C. Chen, Y. Si, C. Zheng, B. Yang, G. Xing, W. Huang, *Adv. Mater.* **2018**, *30*, 1803856.

[18] S. Cai, H. Shi, J. Li, L. Gu, Y. Ni, Z. Cheng, S. Wang, W. W. Xiong, L. Li, Z. An, W. Huang, *Adv. Mater.* **2017**, *29*, 1701244.

[19] N. Gan, X. Wang, H. Ma, A. Lv, H. Wang, Q. Wang, M. Gu, S. Cai, Y. Zhang, L. Fu, M. Zhang, C. Dong, W. Yao, H. Shi, Z. An, W. Huang, *Angew. Chem. Int. Ed.* **2019**. *131*, 14278-14283.

[20] Z. He, H. Gao, S. Zhang, S. Zheng, Y. Wang, Z. Zhao, D. Ding, B. Yang, Y. Zhang, W. Z. Yuan, *Adv. Mater.* **2019**, *31*, 1807222.

[21] Z. Yang, Z. Mao, X. Zhang, D. Ou, Y. Mu, Y. Zhang, C. Zhao, S. Liu, Z. Chi, J. Xu, Y. C. Wu, P. Y.

Lu, A. Lien, M. R. Bryce, *Angew. Chem. Int. Ed.* **2016**, *55*, 2181-2185.
[22] Y. Gong, G. Chen, Q. Peng, W. Z. Yuan, Y. Xie, S. Li, Y. Zhang, B. Z. Tang, *Adv. Mater.* **2015**, *27*, 6195-6201.
[23] Z. Mao, Z. Yang, C. Xu, Z. Xie, L. Jiang, F. L. Gu, J. Zhao, Y. Zhang, M. P. Aldred, Z. Chi, *Chem. Sci.* **2019**, *10*, 7352-7357.
[24] Y. Xie, Y. Ge, Q. Peng, C. Li, Q. Li, Z. Li, *Adv. Mater.* **2017**, *29*, 1606829.
[25] P. Xue, J. Sun, P. Chen, P. Wang, B. Yao, P. Gong, Z. Zhang, R. Lu, *Chem. Commun.* **2015**, *51*, 10381-10384.
[26] C. Li, X. Tang, L. Zhang, C. Li, Z. Liu, Z. Bo, Y. Q. Dong, Y.-H. Tian, Y. Dong, B. Z. Tang, *Adv. Optical Mater.* **2015**, *3*, 1184-1190.
[27] D. Tu, S. Cai, C. Fernandez, H. Ma, X. Wang, H. Wang, C. Ma, H. Yan, C. Lu, Z. An, *Angew. Chem. Int. Ed.* **2019**, *58*, 9129-9133.
[28] K. Zhang, Q. Sun, L. Tang, Y. Wang, X. Fan, L. Liu, S. Xue, W. Yang, *J. Mater. Chem. C* **2018**, *6*, 8733-8737.
[29] Y. Xiong, Z. Zhao, W. Zhao, H. Ma, Q. Peng, Z. He, X. Zhang, Y. Chen, X. He, J. W. Y. Lam, B. Z. Tang, *Angew. Chem. Int. Ed.* **2018**, *57*, 7997-8001.
[30] T. Zhang, H. Gao, A. Lv, Z. Wang, Y. Gong, D. Ding, H. Ma, Y. Zhang, W. Z. Yuan, *J. Mater. Chem. C* **2019**, *7*, 9095-9101.
[31] Z. Mao, Z. Yang, Z. Fan, E. Ubba, W. Li, Y. Li, J. Zhao, Z. Yang, M. P. Aldred, Z. Chi, *Chem. Sci.* **2019**, *10*, 179-184.
[32] D. Tian, Z. Zhu, L. Xu, H. Cong, J. Zhu, *Mater. Horiz.* **2019**, *6*, 1215-1221.
[33] J. Chen, N. U. Rahman, Z. Mao, J. Zhao, Z. Yang, S. Liu, Y. Zhang, Z. Chi, *J. Mater. Chem. C* **2019**, *7*, 8250-8254.
[34] S. Tian, H. Ma, X. Wang, A. Lv, H. Shi, Y. Geng, J. Li, F. Liang, Z. M. Su, Z. An, W. Huang, *Angew. Chem. Int. Ed.* **2019**, *58*, 6645-6649.
[35] J. Yang, X. Zhen, B. Wang, X. Gao, Z. Ren, J. Wang, Y. Xie, J. Li, Q. Peng, K. Pu, Z. Li, *Nat. Commun.* **2018**, *9*, 840.
[36] J. Yang, H. Gao, Y. Wang, Y. Yu, Y. Gong, M. Fang, D. Ding, W. Hu, B. Z. Tang, Z. Li, *Mater. Chem. Front.* **2019**, *3*, 1391-1397.
[37] J. Yang, Z. Ren, B. Chen, M. Fang, Z. Zhao, B. Z. Tang, Q. Peng, Z. Li, *J. Mater. Chem. C* **2017**, *5*, 9242-9246.
[38] S. Kuno, H. Akeno, H. Ohtani, H. Yuasa, *Phys. Chem. Chem. Phys.* **2015**, *17*, 15989-15995.
[39] M. Li, K. Ling, H. Shi, N. Gan, L. Song, S. Cai, Z. Cheng, L. Gu, X. Wang, C. Ma, M. Gu, Q. Wu, L. Bian, M. Liu, Z. An, H. Ma, W. Huang, *Adv. Optical Mater.* **2019**, *7*, 1800820.
[40] Z. Chai, C. Wang, J. Wang, F. Liu, Y. Xie, Y. Z. Zhang, J. R. Li, Q. Li, Z. Li, *Chem. Sci.* **2017**, *8*, 8336-8344.
[41] S. Kuno, T. Kanamori, Z. Yijing, H. Ohtani, H. Yuasa, *ChemPhotoChem* **2017**, *1*, 102-106.
[42] Y. Shoji, Y. Ikabata, Q. Wang, D. Nemoto, A. Sakamoto, N. Tanaka, J. Seino, H. Nakai, T. Fukushima, *J. Am. Chem. Soc.* **2017**, *139*, 2728-2733.
[43] M. Louis, H. Thomas, M. Gmelch, A. Haft, F. Fries, S. Reineke, *Adv. Mater.* **2019**, *31*, 1807887.
[44] C. A. M. Salla, G. Farias, M. Rouzieres, P. Dechambenoit, F. Durola, H. Bock, B. de Souza, I. H. Bechtold, *Angew. Chem. Int. Ed.* **2019**, *58*, 6982-6986.
[45] J. Wei, B. Liang, R. Duan, Z. Cheng, C. Li, T. Zhou, Y. Yi, Y. Wang, *Angew.Chem. Int.Ed.* **2016**, *55*, 15589-15593.
[46] T. Zhang, Z. Zhao, H. Ma, Y. Zhang, W. Z. Yuan, *Chem. Asian J.* **2019**, *14*, 884-889.
[47] B. Chen, X. Zhang, Y. Wang, H. Miao, G. Zhang, *Chem. Asian J.* **2019**, *14*, 751-754.
[48] Z.-Y. Zhang, Y. Liu, *Chem. Sci.* **2019**, *10*, 7773-7778.
[49] S. Hirata, M. Vacha, *J. Phys. Chem. Lett.* **2016**, *7*, 1539-1545.
[50] E. Lucenti, A. Forni, C. Botta, L. Carlucci, C. Giannini, D. Marinotto, A. Previtali, S. Righetto, E. Cariati, *J. Phys. Chem. Lett.* **2017**, *8*, 1894-1898.
[51] H. Bhatia, I. Bhattacharjee, D. Ray, *J. Phys. Chem. Lett.* **2018**, *9*, 3808-3813.
[52] L. Gu, H. Shi, L. Bian, M. Gu, K. Ling, X. Wang, H. Ma, S. Cai, W. Ning, L. Fu, H. Wang, S. Wang, Y. Gao, W. Yao, F. Huo, Y. Tao, Z. An, X. Liu, W. Huang, *nature photon.* **2019**, *13*, 406-411.
[53] M. Fang, J. Yang, X. Xiang, Y. Xie, Y. Dong, Q. Peng, Q. Li, Z. Li, *Mater. Chem. Front.* **2018**, *2*, 2124-2129.